Title
Impaired spatial selectivity and intact phase precession in two-dimensional virtual reality

Journal
Nature Neuroscience, 18(1)

ISSN
1097-6256

Authors
Aghajan, ZM
Acharya, L
Moore, JJ
et al.

Publication Date
2015

DOI
10.1038/nn.3884

Peer reviewed

nature neuroscience

Impaired spatial selectivity and intact phase precession in two-dimensional virtual reality

Zahra M Aghajan[1,2,7], Lavanya Acharya[1,3,7], Jason J Moore[1,4], Jesse D Cushman[1,2], Cliff Vuong[1,2] & Mayank R Mehta[1,2,4–6]

During real-world (RW) exploration, rodent hippocampal activity shows robust spatial selectivity, which is hypothesized to be governed largely by distal visual cues, although other sensory-motor cues also contribute. Indeed, hippocampal spatial selectivity is weak in primate and human studies that use only visual cues. To determine the contribution of distal visual cues only, we measured hippocampal activity from body-fixed rodents exploring a two-dimensional virtual reality (VR). Compared to that in RW, spatial selectivity was markedly reduced during random foraging and goal-directed tasks in VR. Instead we found small but significant selectivity to distance traveled. Despite impaired spatial selectivity in VR, most spikes occurred within ~2-s-long hippocampal motifs in both RW and VR that had similar structure, including phase precession within motif fields. Selectivity to space and distance traveled were greatly enhanced in VR tasks with stereotypical trajectories. Thus, distal visual cues alone are insufficient to generate a robust hippocampal rate code for space but are sufficient for a temporal code.

Dorsal hippocampal neurons fire at elevated rates in restricted regions of space[1,2] when subjects forage randomly in a two-dimensional space, termed a spatial rate code. Distal visual cues are thought to reliably determine this spatial selectivity because changing or rotating them causes corresponding large changes in the spatial tuning of place cells[2,3]. However, the activity of place cells is also influenced by other sensory and motor cues, including specific and nonspecific proximal cues, such as olfactory and somatosensory cues[4–10], and locomotion cues such as optic flow and proprioception, which together with vestibular cues are thought to provide self-motion information for path integration[11–13]. Consistently, lesions of vestibular nuclei disrupt angular tuning of head-direction cells[14] and spatial tuning of hippocampal place cells[15], although lesions of the head-direction cell network, which is thought to provide vestibular input to the hippocampus, do not substantially alter hippocampal spatial selectivity[16]. Additionally, the output of vestibular nuclei suppresses self-motion signals and depends on multisensory stimuli[17]. Indeed, in all the experiments described above, it is difficult to dissociate the contribution of distal visual cues from the contributions of other cues. Thus, the contribution of distal visual cues alone—which are the only spatially informative stimuli in typical human and primate studies of hippocampal activity—to the spatial selectivity of place cells in normal rats remains to be fully explained.

Neural activity is also modulated jointly by theta rhythm and the rat's position within the place field, called theta-phase precession or temporal code[18–21], which is thought to be linked closely to hippocampal spatial selectivity[18]. Nevertheless, phase precession is also seen when rats run in a running wheel without any systematic change in visual cues[22]. Hence, to understand the mechanisms of the hippocampal spatial rate and temporal codes, it is important to determine whether the two can be dissociated during spatial exploration. In addition, dorsal hippocampal neurons are typically active for sustained periods lasting more than 1 second[1,2], even under a variety of conditions[22–25], and this sustained nature of activity has received little attention.

These questions are particularly important to address, as neural mechanisms of navigation in humans and nonhuman primates are studied in stationary subjects for the most part, often in VR[26–28], with only distal visual cues and no vestibular or proximal cues. Under these conditions, hippocampal neurons show only weak spatial selectivity[27–29], an observation that is at apparent odds with the high spatial selectivity seen in studies in freely behaving rodents. Further, an increasing number of functional imaging studies in rodents are being done in head-fixed animals in VR[30].

VR allows for the elimination of spatially informative multisensory, nonspecific cues and minimization of vestibular cues, leaving only distal visual cues to provide reliable spatial information[21,31–33]. All previous neurophysiological studies in rodents in VR have been done in one-dimensional mazes and have found largely intact spatial selectivity. In these environments, visual cues are paired repeatedly with the same set of locomotion cues, such as speed of optic flow and proprioception, which have been hypothesized to have a major role in driving neural responses[11–13,21,34], as evidenced by disto-coding in one-dimensional VR paths[21]. This consistency is removed in random foraging in two-dimensional VR environments where the

[1]W.M. Keck Center for Neurophysics, Integrative Center for Learning and Memory, and Brain Research Institute, University of California at Los Angeles, Los Angeles, California, USA. [2]Department of Physics and Astronomy, University of California at Los Angeles, Los Angeles, California, USA. [3]Biomedical Engineering Interdepartmental Program, University of California at Los Angeles, Los Angeles, California, USA. [4]Neuroscience Interdepartmental Program, University of California at Los Angeles, Los Angeles, California, USA. [5]Department of Neurology, University of California at Los Angeles, Los Angeles, California, USA. [6]Department of Neurobiology, University of California at Los Angeles, Los Angeles, California, USA. [7]These authors contributed equally to this work. Correspondence should be addressed to M.R.M. (mayankmehta@ucla.edu).

Received 12 August; accepted 29 October; published online 24 November 2014; doi:10.1038/nn.3884

same physical location in space can be approached from multiple different directions at different speeds. We thus investigated the contribution of distal visual cues only in determining selectivity in such an experimental setup.

RESULTS

Nature of spatial selectivity of hippocampal responses

We measured hippocampal activity during a two-dimensional random-foraging task in RW and VR[35–37] with similar distal visual cues (**Fig. 1a**). In VR, the rats were body-fixed, i.e., their bodies were held in place, with a harness on a floating ball, allowing for head movements but precluding full-body turns, thus minimizing vestibular cues (Online Methods)[21,36]. Rats quickly learned to avoid the virtual edges entirely on the basis of visual cues[36] and spent a similar amount of time away from the edges and in the center of the platform (**Fig. 1a**) compared to in RW. We measured the activity of 1,066 and 1,238 principal neurons in RW and VR, respectively, in the dorsal CA1 of four rats under a variety of conditions (Online Methods). Neurons fired vigorously in restricted regions of space in RW, as expected (**Fig. 1b**,**c**, **Supplementary Fig. 1a** and **Supplementary Video 1**)[1]. In contrast, the neurons showed little spatial selectivity in VR during random foraging (**Fig. 1b**,**d** and **Supplementary Fig. 1b**).

Across the ensemble, neurons had moderately reduced (25%) mean firing rates but greatly reduced (68%) peak firing rates in VR (**Fig. 2a** and **Supplementary Fig. 2a**). Neurons in VR also had greatly reduced spatial information content (75%), stability (59%), sparsity (42%) and coherence (40%) (**Fig. 2b–d** and **Supplementary Fig. 2b**,**c**) compared to spatially localized, stable and sparse RW rate maps (**Fig. 2c**). Although the mean firing rate was inversely correlated with information content (**Supplementary Fig. 2d**), this large reduction in spatial selectivity cannot be accounted for by differences in mean firing rates in VR and RW, as neurons with similar firing rates had substantially lower spatial selectivity and stability in VR (**Supplementary Figs. 2d**,**e** and **3**). Analysis of relative spatial dynamics between cells measured simultaneously showed that neurons did not maintain consistent spatial relationships with each other in VR, in contrast to in RW (Online Methods and **Supplementary Fig. 4a–d**). We further confirmed this observation using analysis of the cross-covariance of firing rates in time and in distance, which showed little evidence of coactivation or reliable pairing of groups of neurons in VR, in contrast to in RW (**Supplementary Fig. 4e**). These results demonstrate that in VR, neurons did not have place fields that drifted together, nor were they activated in a sequential fashion, in some unknown reference frame.

We also characterized the activity of 258 neurons recorded in both worlds on the same day (**Fig. 1b**). Of these neurons, only 109 (42%) had a mean firing rate above a minimal activity threshold of 0.2 Hz in both worlds. For these neurons, there was a significant correlation between the mean firing rates ($r = 0.21$, $P = 0.03$), but not the peak firing rates ($r = 0.12$, $P = 0.23$), in RW and VR (**Supplementary Fig. 5a**,**b**), although they showed spatial selectivity in RW but not in VR and had uncorrelated rate maps (**Supplementary Fig. 5c**,**d**).

Contribution of task type and locomotion cues

In RW, rats might use a goal-directed strategy to navigate to a food pellet, whereas in VR, there are no reward-predicting cues; such a difference in task type could influence hippocampal activity[12]. To control for this difference, we did a separate experiment in which we measured the activity of 195 neurons from three rats while they ran toward a reward-indicating suspended pillar appearing at random

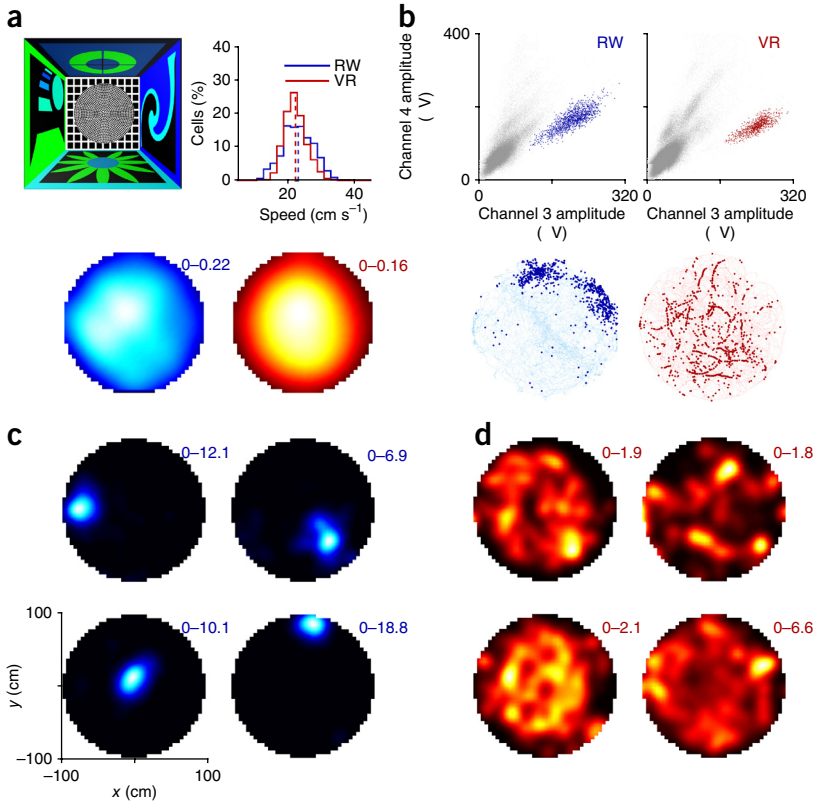

Figure 1 Similar rat behavior but different neural rate maps in two-dimensional RW and VR. (**a**) Top left, top-down schematic view of the RW and VR mazes showing a 200-cm-diameter elevated platform centered in a 300 cm × 300 cm room with distinct visual cues on the walls. Top right, mean running speed at the time of occurrence of spikes (excluding speeds <5 cm s^{-1}) was slightly reduced (3%, $P = 0.0005$) in VR (22.40 ± 0.13 cm s^{-1}, red, $n = 719$ cells from 4 rats) compared to RW (23.27 ± 0.16 cm s^{-1}, blue, $n = 1,066$ cells from 4 rats). Bottom, percentage of time spent in all parts of the maze averaged across all rats, showing that rats spent comparable time away from the edges in RW (left) and VR (right). (**b**) Top, scatter plots of the peak amplitude of a spike (gray dots) measured simultaneously on two channels (channels 3 and 4) of a tetrode in RW and VR. Colored dots are spikes from the same isolated neuron recorded on the same day in the two worlds. Bottom, position of the rat in RW and VR at the time of occurrence of the spikes (darker dots) from the corresponding neurons (top) overlaid on the trajectory of the rat (lighter trace). (**c**) Spatial rate maps of four neurons in RW. (**d**) Same as **c** but in VR. All data throughout all figures and figure legends are expressed as the mean ± s.e.m., unless otherwise noted. Throughout all figures, dashed vertical lines in histograms indicate the mean values of the corresponding distributions. In all figures, blue indicates RW and red indicates VR, numbers above images indicate the ranges, and lighter shades indicate higher values. In all figures, statistical significance was calculated by Wilcoxon rank-sum test, unless otherwise noted.

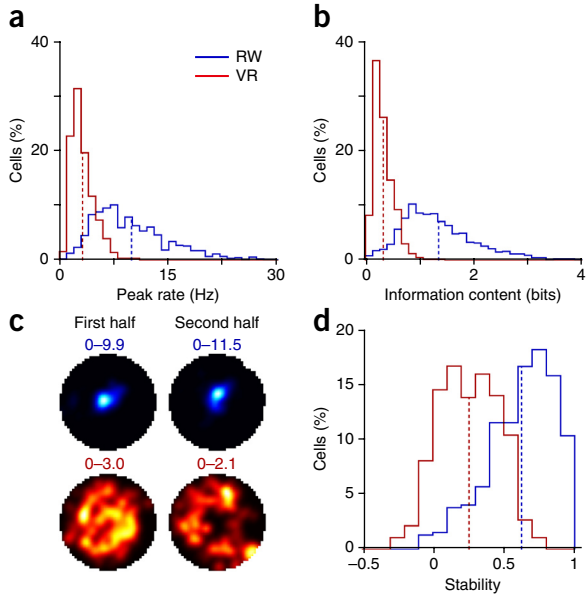

Figure 2 Reduced activity, spatial selectivity and stability of rate maps in VR. (**a**) The peak firing rates of neurons were 68% ($P = 1.1 \times 10^{-161}$) smaller in VR (3.19 ± 0.07 Hz, $n = 719$ cells from 4 rats) compared to RW (9.90 ± 0.18 Hz, $n = 1{,}066$ cells from 4 rats). (**b**) The spatial information content in VR (0.33 ± 0.01 bits) was 75% ($P = 1.1 \times 10^{-183}$) lower than that in RW (1.35 ± 0.02 bits). (**c**) Rate maps of a neuron during the first and second halves of a session in RW and VR. (**d**) The stability of rate maps in VR (0.26 ± 0.01) was significantly reduced (difference = 0.37, $P = 1.2 \times 10^{-124}$) compared to in RW (0.63 ± 0.01).

locations in VR (**Fig. 3a** and Online Methods)[36]. The excess path length of the rats' trajectory between rewards was significantly shorter during this random-pillar task (69%, $P = 6.1 \times 10^{-4}$) than during the random-foraging task, which is indicative of a goal-directed strategy (**Supplementary Fig. 6a**,**b**). There was no substantial difference in spatial selectivity between the two types of task in VR (**Fig. 3b** and **Supplementary Video 2**), which argues that the loss of spatial selectivity was not due to differences in task type. Hence, for subsequent comparisons between RW and VR, we combined data from the random-foraging and random-pillar tasks.

The loss of spatial selectivity in two-dimensional VR is in stark contrast to not only that in two-dimensional RW but also to that in previous studies in one-dimensional VR[21,31–33] in which clear spatial selectivity was found. To test whether spatial selectivity could exist in the same two-dimensional VR environment without the vestibular cues present in RW, we did another experiment in which the task type was similar to the random-pillar task but the reward-indicating pillars appeared systematically at fixed locations (**Fig. 3c**,**d** and Online Methods). In the first variant, pillars appeared at two fixed but alternating positions in VR (**Supplementary Fig. 6a**). Because rats ran in more stereotyped trajectories, locomotion cues—such as step counting from the previous reward and speed of optic flow—were made spatially informative, as the same cues occurred repeatedly at the same positions across the task. Consequently, unique locomotion cues were paired repeatedly with distinct distal visual cues at each position (**Fig. 3c**). Spatially selective neural responses appeared in this systematic-pillar task with significantly enhanced spatial information content and rate map sparsity compared to random foraging in VR (**Fig. 3e**,**f**). Although some neurons had a focused place field in only one direction of movement, or arm, similarly to place cells in RW, others spiked on both arms (**Fig. 3e** and **Supplementary Fig. 7a**), which we investigated in detail and describe below.

To rule out the possibility that spatial selectivity arose simply from alternating contexts in two movement directions or that the rat did not traverse a large portion of the maze, we did another variant of the systematic-pillar task in which the reward-indicating pillars appeared sequentially at the vertices of an equilateral triangle (Online Methods). Here the rats walked repeatedly along the same paths while covering a greater fraction of the two-dimensional maze, and because adjacent arms were rotated 120° with respect to each other rather than 180°, the visual scene was more similar along different arms than in the two-pillar task (**Supplementary Fig. 6a**).

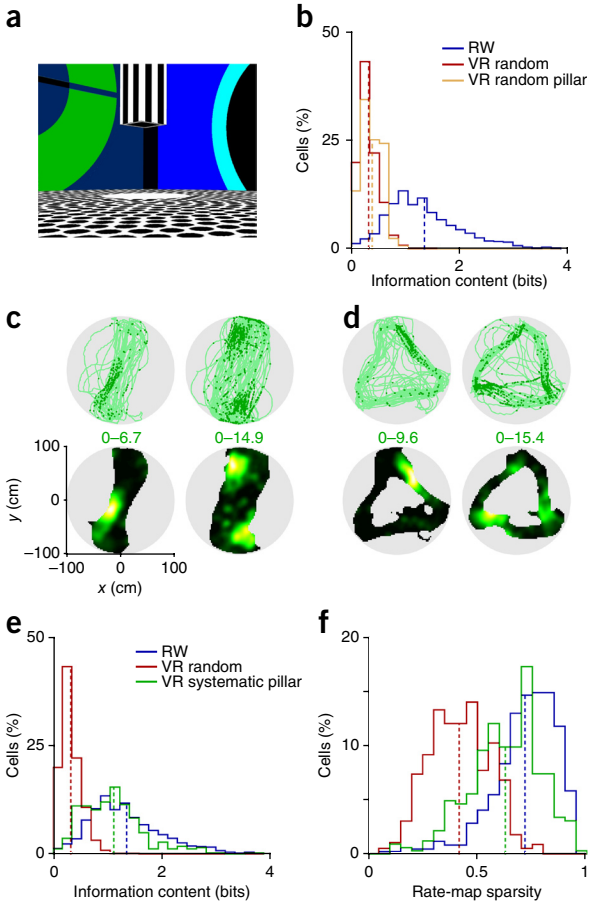

Figure 3 Dependence of spatial selectivity on task type and locomotion cues. (**a**) Schematic of a maze in which the reward location is indicated by a pillar suspended in VR (VR random pillar). (**b**) The spatial information content in VR random pillar (0.39 ± 0.02 bits, $n = 195$ cells from 3 rats) was only slightly (16%, $P = 1.6 \times 10^{-4}$) larger than in VR random (0.33 ± 0.01 bits) and was still substantially smaller (71%, $P = 1.1 \times 10^{-55}$) than in RW (1.35 ± 0.02 bits). (**c**) Top, trajectory of the rat (light green trace) and position of the rat at the time of occurrence of spikes (darker dots) for two example neurons during consistent paths between two fixed reward locations on a two-pillar task. Bottom, rate maps corresponding to the neurons shown above. (**d**) Same as **c** but on a three-pillar task. Gray regions indicate positions the rat did not sample for a sufficient amount of time. (**e**) The spatial information content in VR with systematic pillars (1.11 ± 0.03 bits, $n = 324$ cells from 3 rats) was significantly larger than in VR random (70%, $P = 1.0 \times 10^{-101}$) and was only slightly smaller than in RW (17%, $P = 5.3 \times 10^{-8}$). (**f**) The spatial sparsity in VR systematic pillar (0.63 ± 0.01) was significantly greater (34%, $P = 4.7 \times 10^{-63}$) than in VR random (0.42 ± 0.01) and was close (12% less, $P = 4.6 \times 10^{-20}$) to that in RW (0.72 ± 0.01).

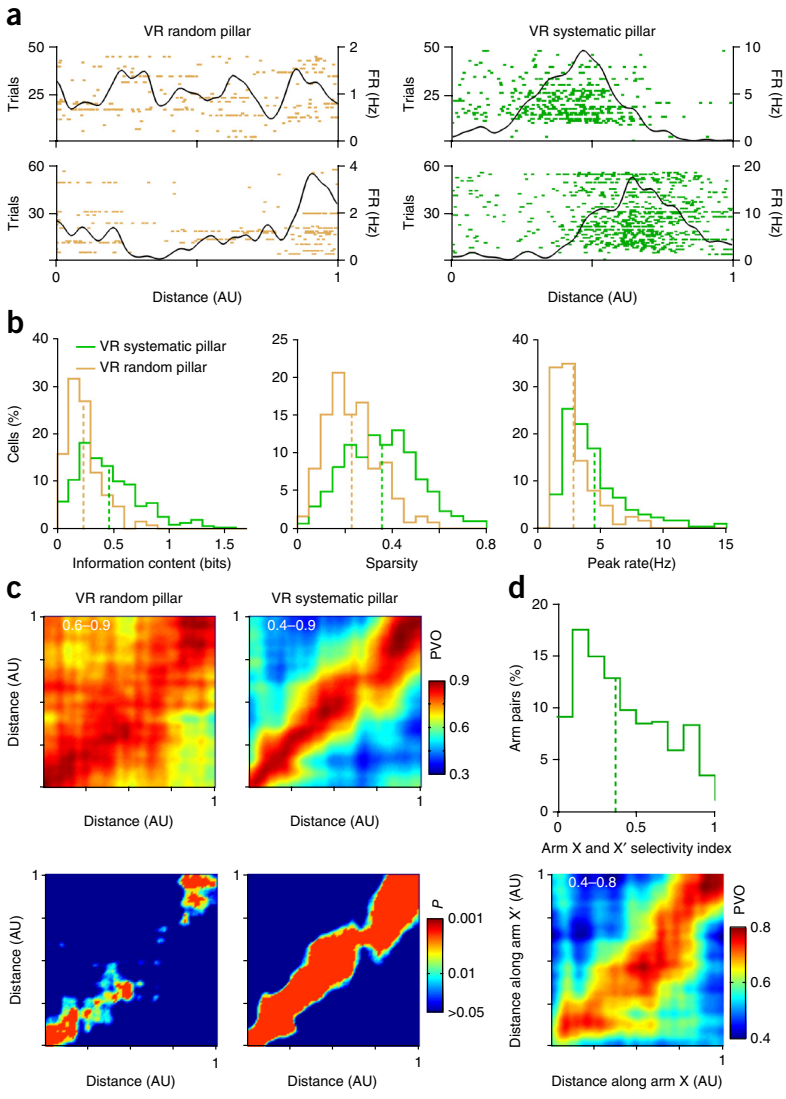

Figure 4 Selectivity to distance traveled in VR goal-directed tasks. (**a**) Firing rate (FR) of cells as a function of normalized distance traveled across trials. In the VR random-pillar task, many cells exhibited random firing (top left), whereas some had elevated firing at the beginnings and ends of trials (bottom left). In the VR systematic-pillar task, neurons had focused firing at specific distances along the different arms (right). AU, arbitrary units. (**b**) Left, information content in linearized paths in the VR random-pillar task (0.24 ± 0.01 bits, $n = 127$ cells from 3 rats) was significantly lower (49%, $P = 1.2 \times 10^{-17}$) than in the VR systematic-pillar task (0.47 ± 0.02 bits, $n = 310$ cells from 3 rats). Center, similarly, sparsity of the linearized firing rate maps in the VR random-pillar task (0.23 ± 0.01) was significantly reduced (36%, $P = 5.9 \times 10^{-16}$) compared to in the VR systematic-pillar task (0.36 ± 0.01). Right, peak firing rates were 36% ($P = 3.1 \times 10^{-15}$) smaller in the VR random-pillar task (2.89 ± 0.14 Hz) compared to in the VR systematic-pillar task (4.55 ± 0.15 Hz). (**c**) PVO in the VR random-pillar (top left) and VR systematic-pillar (top right) tasks. The range of overlap is indicated by the numbers at the top left corners. The bottom row depicts the significance levels for the corresponding PVO presented in the top row. The significant diagonal area indicates selectivity to distance on an ensemble level. (**d**) Top, for different arm pairs with minimal activity on at least one arm (mean rate >0.5 Hz, $n = 625$ arm pairs from 3 rats), the arm selectivity index (0.37 ± 0.01) quantifies the likelihood of firing on one arm (index >0.5) compared to on multiple arms (index ≤0.5). X and X′ refer to distinct arms in the arm pair of interest. Bottom, PVO for arm pairs with arm selectivity index below 0.5 ($n = 431$ arm pairs from 3 rats).

Spatially selective, stable responses also appeared in this task, which were significantly greater than those in the two-dimensional random-foraging tasks in VR but were comparable to those in two-dimensional random foraging in RW (**Fig. 3d–f** and **Supplementary Figs. 6c** and **7b**). Here too, some neurons spiked on only one arm of the triangle (**Supplementary Video 3**), similarly to RW place cells, whereas others spiked along multiple arms (**Supplementary Fig. 8a**,**b** and **Supplementary Video 4**).

In both of the systematic-pillar experiments, vestibular cues remained minimal and spatially uninformative during turns, yet spatial selectivity was comparable to that in random foraging in RW. Further, in systematic-pillar tasks and the random-pillar task, the path between two successive reward locations was not always direct but instead often deviated from the optimal, straight-line path (**Supplementary Fig. 6a**). This departure, or excess path length, was comparable in both the systematic- and random-pillar tasks (**Supplementary Fig. 6b**), indicating similar levels of goal-directed behavior and demonstrating that differences in departure from the shortest paths do not underlie the observed differences in spatial selectivity. Thus, task type cannot explain the differences in spatial selectivity observed under different conditions in RW and VR.

The presence of firing on multiple arms in the systematic-pillar tasks (**Fig. 3c** and **Supplementary Fig. 8a**) suggests that neurons might be coding for the distance traveled along the paths. If this is the case, it raises the possibility that neurons in the random-pillar task might also exhibit similar coding despite their lack of two-dimensional spatial selectivity (**Supplementary Fig. 8a**). The fact that the beginning and end of a trial were clearly delineated by the visible pillars in all goal-directed tasks allowed us to test these possibilities by quantifying the activity of neurons as a function of normalized distance traveled along each path, subsequently referred to as distance (Online Methods).

In the random-pillar task, many but not all neurons exhibited random firing both on linearized paths and in two-dimensional space (**Fig. 4a** and **Supplementary Fig. 8a**). In contrast, a majority of neurons in the systematic-pillar tasks often fired at the same distance (**Fig. 4a** and **Supplementary Fig. 8a**). Linearized rate maps in the random-pillar tasks had lower information content (49%), sparsity (36%) and peak rate (36%) compared to those in the systematic-pillar task (**Fig. 4b**), although a small number of neurons in the random-pillar task had measures comparable to those in the systematic-pillar task (**Fig. 4b**). We further characterized this selectivity on a population level by computing the population vector overlap (PVO) between the firing rates of two groups of randomly selected paths for each cell (Online Methods). Whereas the significant overlap in the random-pillar task was limited to regions near the beginnings and ends of trials, it was present at all distances in the systematic-pillar tasks (**Fig. 4c**).

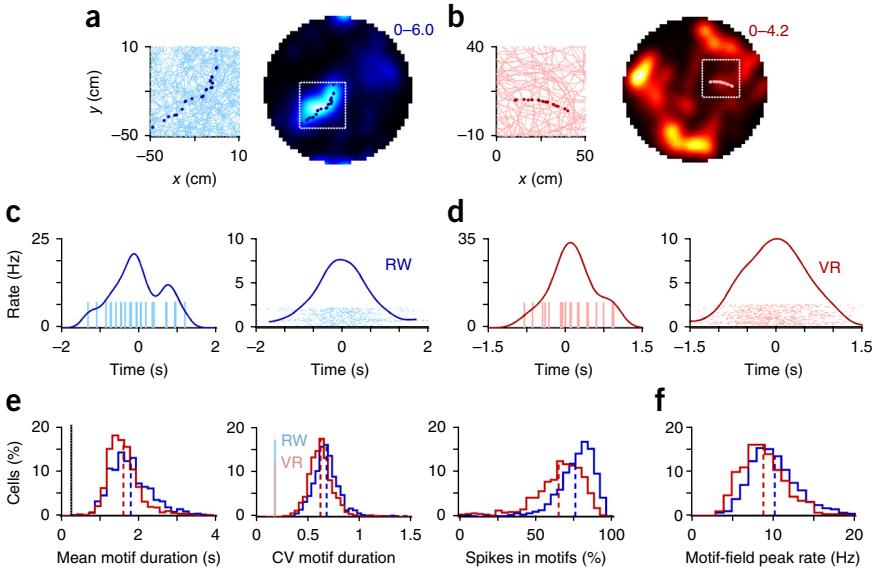

Figure 5 Similar hippocampal motifs and motif fields in RW and VR. (**a**) Spike positions of an example motif from a cell overlaid on a segment of the rat's trajectory (left) and firing rate map (right) in RW. (**b**) Similar plot as those in **a** but in VR. (**c**) Left, motif firing rate as a function of time and individual spike times (vertical lines) for the same motif as in **a**. Right, motif-field firing rate as a function of time. Spikes from individual motifs are depicted in the raster plot, aligned around the centers of mass of the motifs to form the motif field. In other words, each row of the raster plot represents an individual pass through the motif field. (**d**) Same as **c** but in VR. (**e**) Left, mean motif durations of cells with at least five motifs (1,064 out of 1,066 in RW and 911 out of 914 in VR, comprising 719 cells from VR random from 4 rats and 195 cells from VR random pillar from 3 rats) were comparable in RW (1.82 ± 0.02 s) and VR (1.63 ± 0.02 s) but were slightly smaller in VR (7%, $P = 2.2 \times 10^{-12}$). The shortest allowed motif duration (dashed vertical black line) was much smaller than the ensemble average. Center, the coefficients of variation (CV) of motif durations within each cell were comparable in RW (0.69 ± 0.00) and VR (0.63 ± 0.01) but were slightly lower in VR (8%, $P = 5.7 \times 10^{-20}$); both were much greater than the CV of the distributions in the plot to the left (solid vertical lines). Right, although a majority of spikes were contained within motifs in RW (75.90 ± 0.47%) and VR (64.99 ± 0.63%), there was a small reduction these numbers in VR (14%, $P = 1.2 \times 10^{-51}$). (**f**) The peak firing rates of motif fields in VR (8.85 ± 0.10 Hz) were only slightly smaller (13%, $P = 2.1 \times 10^{-17}$) than those in RW (10.22 ± 0.11 Hz).

We additionally tested whether the neurons spiked at the same distance on two different arms of the triangle located in different parts of the maze. We quantified the number of cells that fired on multiple arms by calculating the arm selectivity index (**Fig. 4d** and Online Methods). For cells that were active on multiple arms (index <0.5), which constituted a majority of the cells, PVO analysis between the rate maps of the two arms revealed significant overlap at all distances, indicative of a robust disto-code, notably on nonoverlapping paths (**Fig. 4d** and **Supplementary Fig. 8b**,**c**). These results, together with the differences in two-dimensional spatial selectivity presented above, suggest that repeated traversals along the same path, such as in the systematic-pillar task, are crucial for generating robust spatial selectivity and selectivity to distance, a generalization of the disto-code.

Hippocampal motifs and phase precession

In RW, neurons generated long spike sequences lasting about 2 seconds as rats traversed through well-defined place fields (**Fig. 5a** and **Supplementary Fig. 1a**). Surprisingly, despite having no clearly defined place fields, neurons in VR also fired similarly long spike sequences, which appeared as streaks of spikes (**Fig. 5b** and **Supplementary Fig. 1b**). We term these long spike sequences hippocampal motifs, identified as time periods in which a neuron achieved a peak firing rate of at least 5 Hz and maintained a firing rate above 10% of that peak for at least 300 ms. We aligned all individual motifs from a cell around their center of mass and aggregated them to obtain the cell's motif field (**Fig. 5c**,**d** and Online Methods).

Motif properties, including mean motif duration, fraction of spikes contained in motifs, mean firing rate and peak firing rate, were comparable in the two worlds (**Fig. 5e** and **Supplementary Fig. 9a**,**b**) and were far greater than expected by chance, particularly when accounting for the lower mean rates in VR (**Supplementary Fig. 9c**,**i**,**j**). Although for any given cell, the motif durations were quite variable in either world, (**Fig. 5e**), mean motif durations across all cells displayed small variability (**Fig. 5e**). Whereas the variability in motif durations in RW could be due to a varying amount of time spent within the place field in each traversal, the motif durations were equally variable in VR (**Fig. 5e**), with little spatial selectivity, suggestive of an intrinsic, network-wide mechanism for motif generation. Neurons with a larger fraction of spikes within motifs had greater information content (**Supplementary Fig. 9d**) and mean firing rates (**Supplementary Fig. 9c**), which is in contrast to the inverse correlation between information content and mean firing rate seen across all cells when all spikes were included (**Supplementary Fig. 2d**). Spiking within motifs, as opposed to isolated spiking, may therefore serve to group otherwise random and noninformative spikes into more informative clusters.

Analysis of motif fields (**Fig. 5c**,**d**) showed similar results, with motif fields having similar durations, mean rates and peak rates in RW and VR (**Fig. 5f** and **Supplementary Fig. 9e**,**f**), in contrast to the smaller peak rates in spatial rate maps seen in VR (**Fig. 2a**). Neurons active in RW and VR on the same day also had motif fields with similar durations and peak firing rates (**Supplementary Fig. 9g**,**h**).

In spite of the impaired rate code, do the motifs show a temporal code[18–21,31,33]? Because of the absence of clear place fields in VR, we quantified the quality of phase precession within motif fields by computing the circular linear correlation (Online Methods) between the time spent within the motif field and the theta phase of spikes. In RW, 80% of neurons showed significant phase precession within motif fields (**Fig. 6a**,**b**). This number was reduced to 40% in VR but was still far greater than expected by chance (**Fig. 6a**,**b** and Online Methods). For cells with significant precession, the quality of precession was comparable in both worlds, although it was slightly reduced in VR (**Fig. 6b**). For all cells, we also computed the difference between the period of theta modulation of spikes and the local field potential (LFP) theta period[18,20,38]. A majority of cells in RW (83%) and VR (78%) had a longer LFP theta period than their spike theta period, which is indicative of intact temporal coding in VR (**Fig. 6c**). This is especially notable because the LFP theta had greater peak theta power and reduced theta frequency in VR (**Supplementary Fig. 10a–c**). The preferred theta phase of neurons was also significantly different and

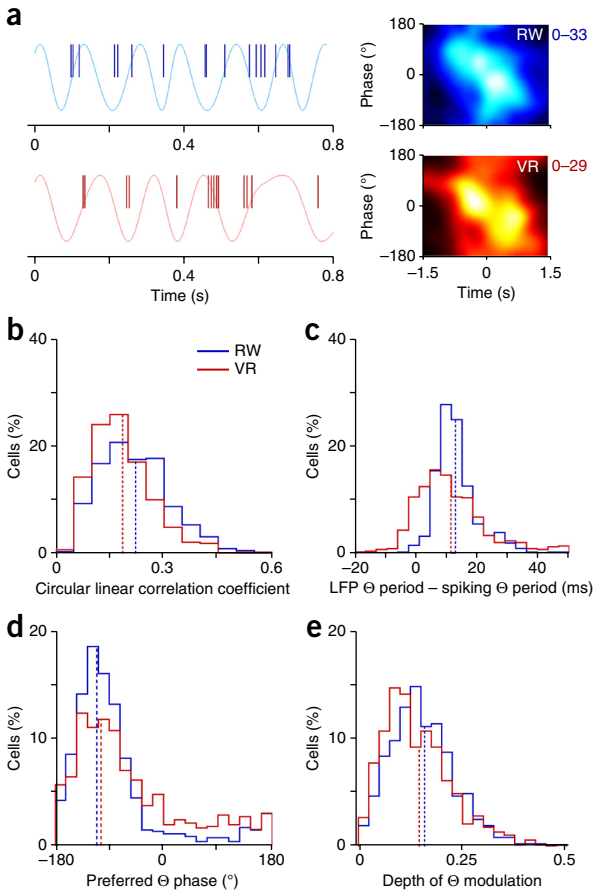

Figure 6 Intact but variable phase coding in VR. (**a**) Left, sample LFP theta traces filtered in the theta band (4–12 Hz) in RW (top) and VR (bottom) recorded from the same electrode on the same day. Spikes from the same cell (vertical lines) in RW and VR occur at earlier phases on subsequent theta cycles. Right, motif fields in RW and VR show clear phase precession. (**b**) 80.03% and 40.52% of cells showed significant phase precession in RW and VR, respectively. For these cells, the quality of phase precession in VR cells (0.185 ± 0.004, $n = 365$ cells from 4 rats) was slightly reduced (13%, $P = 1.9 \times 10^{-11}$) compared to in RW (0.221 ± 0.003, $n = 852$ cells from 4 rats). (**c**) Difference in LFP theta period and spiking theta period computed from the autocorrelation of LFP and spikes shows comparable but reduced (11%, $P = 4.6 \times 10^{-9}$) and more variable temporal coding in VR (11.38 ± 0.46 ms (mean ± s.d.)) compared to RW (12.85 ± 0.23 ms (mean ± s.d.)). (**d**) The preferred theta phase of spikes was shifted closer to the theta peak (6%, $P = 0.001$, Kuiper's test) in VR (–103.70 ± 2.29°) and was also more variable (s.d. 61.40°) compared to in RW (–110.58 ± 1.72°, s.d. 56.15°). (**e**) The degree of phase locking (depth of modulation) was similar in VR (0.15 ± 0.09) and RW (0.16 ± 0.09), although was slightly reduced (8%, $P = 8.5 \times 10^{-5}$) in VR.

more variable in VR compared to RW (**Fig. 6d**), yet neurons showed similar degrees of theta-phase locking in both worlds (**Fig. 6e**).

DISCUSSION

These results provide the first measurements, to our knowledge, of rodent hippocampal CA1 neuronal activity during random foraging in a two-dimensional body-fixed VR environment in which only distal visual cues provide reliable spatial information. We found five key results: a profound loss of spatial selectivity during random foraging in VR; intact spatial selectivity when both location-specific locomotion cues and distal visual cues were repeatedly experienced together during the systematic-pillar tasks; weak but significant selectivity to distance traveled in the random-pillar task and strong distance selectivity in the systematic-pillar tasks; comparable motif dynamics in RW and VR; and intact temporal code within motif fields in VR.

We speculate that the motif-generation mechanisms are intrinsic to the entorhinal-hippocampal network because, unlike most afferent sensory cortices showing punctate neural responses, hippocampal neurons showed ~2-s-long sustained responses in both RW and VR, despite the absence of spatial selectivity in the latter world. These sustained responses could enable the entorhinal-hippocampal system to predict the rat's future location on the basis of recent experience[39] by exploiting the continuity of space and locomotion, thus reducing computational load.

The motif generation mechanism is probably network-wide rather than cell specific, as the variability in motif durations on a population level is small compared to the individual neuronal level, motif-field properties are correlated between RW and VR, and theta-scale dynamics are intact in VR motif fields. Whereas previous studies have shown intact phase precession without a change in position-defining cues in a working memory task[22], our results demonstrate instead that phase precession can exist without a rate code when spatially informative cues are changing with minimal memory demand. Increased preferred theta-phase variability could arise through a rate-phase transformation[19] and a reduced excitatory drive in VR due to a lack of repeatedly paired sensory and motor cues, as described below. The underlying network mechanism could thus generate motif-like activity under a variety of conditions, including hippocampal place cells from normal subjects[21,31,33] and transgenic mice with taupathy[40], entorhinal cortical grid cells[38], episode or time cells during wheel or treadmill running[22,23], neural activity during rapid eye movement sleep[41] and neural activity during free recall in humans[42].

Motifs could originate from several parts of the entorhinal-hippocampal network. The recurrent CA3 network could generate motif-like activity, which might cause the observed ~2-s delayed responses of the hippocampal ensemble activity pattern to sudden changes in visual cues[24]. Alternatively, the motifs could arise in the medial entorhinal cortex, where neurons show motif-like activity lasting several seconds and robustly driving the CA1, even in anesthetized or sleeping animals[43]. Accordingly, sustained spiking in consecutive theta cycles was reduced, indicative of diminished motifs, in a GluA1 transgenic mouse with diminished distal dendritic inputs, which typically originate in the entorhinal cortex[44]. Motif-field durations could also be modulated by the temporal integration properties of the h current[45] to generate a dorsoventral gradient of field sizes.

Although intact motifs and phase precession are present in VR with distal visual cues alone, we found a large reduction in spatial selectivity during two-dimensional random-foraging and random-pillar tasks in a body-fixed VR. This finding demonstrates that distal visual cues alone are not sufficient to generate spatially localized place fields[2,3]. In contrast, spatial selectivity was present in the systematic-pillar tasks but not the random-pillar task. Although diminished vestibular cues during random foraging in VR might account for reduced spatial selectivity compared to during random foraging in RW, it is inconsistent with the presence of spatial selectivity in the systematic-pillar tasks, in which the nature of paths and resulting vestibular cues are similar to those in the random-pillar task. Further, vestibular lesions caused substantial behavioral deficits, reductions in theta power and unaltered peak firing rates[15,46], all of which are in contrast to our data. These results suggest that the repeated pairing of cues, or lack thereof, is the key reason for the difference in two-dimensional spatial selectivity.

The difference in spatial selectivity between the random-pillar and systematic-pillar tasks is also consistent with previous studies demonstrating that the precise nature of paths (random or systematic) can strongly affect the hippocampal spatial representation[12,47].

Whereas two-dimensional spatial selectivity was equally poor in the random-foraging and random-pillar tasks in VR, the beginnings and ends of trials were well defined for the rats in the latter task, thus allowing for an analysis of selectivity to distance traveled. Neurons in the random-pillar task showed a small but significant degree of selectivity to the beginnings and ends of trials. In the systematic-pillar task, when we paired locomotion and visual cues repeatedly, this selectivity was strengthened and extended to the middle of the paths. Restricting the analysis to cells that fired on at least two nonoverlapping arms on the three-pillar task revealed that these cells exhibited a disto-code[21], which is a specific case of the more general distance selectivity observed in the goal-directed tasks.

We conjecture that repeated pairing of different streams of input could generate robust associations between them through rapid Hebbian synaptic plasticity, resulting in stable spatial representations[48] and increased firing rates[19,48–50]. Under this model, during random foraging in RW, distal visual cues are paired repeatedly with the same constellation of proximal cues at each location, resulting in a place code. In contrast, in two-dimensional random foraging in VR with or without pillars, the distal visual cues are not paired repeatedly with any other cue, leading to a lack of spatial selectivity. Contrary to our VR system and results, a recent study found that during two-dimensional random foraging in a VR system allowing full, 360° body rotation[35,37], hippocampal neurons showed intact spatial selectivity[37]. This result could arise solely from the presence of a larger range of vestibular cues, which were diminished in our study; however, this explanation is incompatible with the presence of spatial selectivity in our tasks involving systematic paths. Two alternate possibilities are provided by our repeated pairing model. First, as rats turned their entire bodies in that study, they rotated with respect to both VR visual cues and RW multisensory cues, leading to a consistent pairing between the two. In agreement with this hypothesis, the activities of a large number of cells were influenced by the RW frame of reference in that study[37]. Second, consistent pairing between vestibular cue-based signals, such as the activity of head-direction cells, and visual cues could be sufficient but not necessary to generate spatial selectivity in VR. Once such a multisensory pairing–induced representation of space is established, it can then be governed by visual cues[2,3,37]. Further studies will be needed to dissociate these possibilities.

According to our model, spatial selectivity arises both in systematic-pillar tasks and on one-dimensional VR tracks because of the repeated pairing between distal visual cues and locomotion cues along systematic paths. Neurons with stronger inputs from distal visual cues would exhibit a place code, whereas those with stronger inputs from locomotion cues would exhibit a disto-code[21]. Further, the overall reduction in the number of sensory and motor cues that are systematically paired could contribute to the large reduction in neural activity in VR[21]. Alternatively, instead of pairing across multiple modalities, pairing in linear paths could potentially occur between adjacent elements within a repeated sequence of cues from a single modality. Consistently, systematic acceleration and deceleration at the beginnings and ends of linearized paths in the random-pillar task could give rise to selectivity in those regions.

Although we characterized distance selectivity as a function of position along the path, neural firing might be influenced by other factors as well. Selectivity near the end of the path could be driven by reward expectancy or the pillar; selectivity near the beginning of the path might be modulated by the recent delivery of reward. These salient episodes associated with entering or leaving a reward zone are present and repeated in all goal-directed tasks, which could result in selectivity to the beginnings and ends of paths even in the random-pillar task. We speculate that these episodes might become linked together by Hebbian synaptic plasticity in the systematic-pillar task by the same mechanism discussed above, thus extending selectivity to the entire length of the path. Further studies will be needed to fully determine the role of episodic memory in these tasks.

Our results may raise the concern that spatial selectivity is impaired during random foraging in VR because the rats are not paying attention to the visual cues present in VR. Although this factor cannot be ruled out entirely, we find it to be unlikely for a number of reasons. First, in both RW and VR, the rats are not required to pay attention to the distal visual cues, yet there is spatial selectivity in RW. Second, rats in VR avoid the edges of the virtual table, which is defined only visually. Third, many neurons in the systematic-pillar tasks fire in only a small portion of one segment of the path, which is differentiated from the other segments only by the direction-specific constellation of distal visual cues. Further, in the same virtual maze apparatus with qualitatively similar visual cues, the rats were able to navigate to a hidden reward zone from multiple starting locations, analogous to in the water maze navigation task[36], using only distal visual cues, showing that rats could see the stimuli and navigate based on them. Additional studies will be needed to determine the nature of spatial selectivity in this task.

The repeated pairing model is compatible with many findings, including place cell remapping after a change in the relationship between locomotion cues and distal visual cues[12], altered spatial selectivity after changes in distal[3,6] or proximal cues[4–9] and instability of place fields after maze cleaning between sessions[7]. In each of these cases, place cells remap but spatial selectivity remains intact, presumably because new associations are formed as cues are paired repeatedly in new configurations. It will be important for future studies to determine whether different pairings are equally viable or whether there is a hierarchy such that certain inputs are more or less effective at contributing to spatial selectivity.

In summary, internally generated and temporally coded motifs represent activity patterns on behavioral timescales and are localized by the repeated experience of multiple location-specific sensory and motor cues. Some selectivity to distance traveled exists near the beginnings and ends of paths even in the absence of spatial selectivity, but repeated pairing strengthens this selectivity and extends it to the entire length of the path. The impaired spatial selectivity in rats in two-dimensional VR is similar to the weak spatial selectivity seen in human studies, in which such pairings are absent as well. Recent studies have shown that a sufficiently large pool of hippocampal neurons can provide accurate spatial information despite impaired spatial selectivity in one-dimensional environments[44]; such a distributed coding mechanism might also allow rodents and humans to solve spatial tasks in two-dimensional VR. Our results suggest that in human and primate studies in VR, repeated pairing of a rich variety of stimuli, especially between motor and visual cues, could enhance neural activity and spatial selectivity. These results bridge the gap between rodent and human studies by showing that distal visual cues alone are insufficient to generate robust spatial selectivity, but even with an impaired rate code, temporally coded motifs are intact, probably generated by intrinsic network mechanisms.

METHODS

Methods and any associated references are available in the online version of the paper.

Note: Any Supplementary Information and Source Data files are available in the online version of the paper.

ACKNOWLEDGMENTS

We thank F. Quezada and B. Popeney for help with behavioral training, F. Quezada for help with spike sorting, N. Agarwal for help with electrophysiology, B. Willers for help with the analyses, P. Ravassard and A. Kees for help with surgeries, technical support and manuscript comments, D. Aharoni for help with hardware and the participants of the Kavli Institute for Theoretical Physics workshop on 'Neurophysics of Space, Time and Learning' for discussions. This work was supported by grants to M.R.M. from the US National Institutes of Health (5R01MH092925-02) and the W.M. Keck foundation. Results presented in this manuscript were uploaded on a preprint server BioRxiv in December 2013 at http://dx.doi.org/10.1101/001636.

AUTHOR CONTRIBUTIONS

L.A., J.D.C., Z.M.A. and M.R.M. designed the experiments. L.A., C.V. and J.D.C. performed the experiments. Z.M.A. and J.J.M. performed analyses with input from M.R.M. Z.M.A., L.A., J.J.M. and M.R.M. wrote the manuscript with input from other authors.

COMPETING FINANCIAL INTERESTS

The authors declare no competing financial interests.

1. O'Keefe, J. & Dostrovsky, J. The hippocampus as a spatial map. Preliminary evidence from unit activity in the freely-moving rat. *Brain Res.* **34**, 171–175 (1971).
2. O'Keefe, J. & Nadel, L. *The Hippocampus as a Cognitive Map* (Clarendon Press, 1978).
3. Muller, R.U. & Kubie, J.L. The effects of changes in the environment on the spatial firing of hippocampal complex-spike cells. *J. Neurosci.* **7**, 1951–1968 (1987).
4. Shapiro, M.L., Tanila, H. & Eichenbaum, H. Cues that hippocampal place cells encode: dynamic and hierarchical representation of local and distal stimuli. *Hippocampus* **7**, 624–642 (1997).
5. Knierim, J.J. Dynamic interactions between local surface cues, distal landmarks, and intrinsic circuitry in hippocampal place cells. *J. Neurosci.* **22**, 6254–6264 (2002).
6. O'Keefe, J. & Conway, D.H. Hippocampal place units in the freely moving rat: why they fire where they fire. *Exp. Brain Res.* **31**, 573–590 (1978).
7. Save, E., Nerad, L. & Poucet, B. Contribution of multiple sensory information to place field stability in hippocampal place cells. *Hippocampus* **10**, 64–76 (2000).
8. Battaglia, F.P., Sutherland, G.R. & McNaughton, B.L. Local sensory cues and place cell directionality: additional evidence of prospective coding in the hippocampus. *J. Neurosci.* **24**, 4541–4550 (2004).
9. Anderson, M.I. & Jeffery, K.J. Heterogeneous modulation of place cell firing by changes in context. *J. Neurosci.* **23**, 8827–8835 (2003).
10. Aikath, D., Weible, A.P., Rowland, D.C. & Kentros, C.G. Role of self-generated odor cues in contextual representation. *Hippocampus* **24**, 1039–1051 (2014).
11. Gothard, K.M., Skaggs, W.E. & McNaughton, B.L. Dynamics of mismatch correction in the hippocampal ensemble code for space: interaction between path integration and environmental cues. *J. Neurosci.* **16**, 8027–8040 (1996).
12. Markus, E.J. *et al.* Interactions between location and task affect the spatial and directional firing of hippocampal neurons. *J. Neurosci.* **15**, 7079–7094 (1995).
13. Terrazas, A. *et al.* Self-motion and the hippocampal spatial metric. *J. Neurosci.* **25**, 8085–8096 (2005).
14. Stackman, R.W. & Taube, J.S. Firing properties of head direction cells in the rat anterior thalamic nucleus: dependence on vestibular input. *J. Neurosci.* **17**, 4349–4358 (1997).
15. Stackman, R.W., Clark, A.S. & Taube, J.S. Hippocampal spatial representations require vestibular input. *Hippocampus* **12**, 291–303 (2002).
16. Calton, J.L. *et al.* Hippocampal place cell instability after lesions of the head direction cell network. *J. Neurosci.* **23**, 9719–9731 (2003).
17. Angelaki, D.E. & Cullen, K.E. Vestibular system: the many facets of a multimodal sense. *Annu. Rev. Neurosci.* **31**, 125–150 (2008).
18. O'Keefe, J. & Recce, M.L. Phase relationship between hippocampal place units and the EEG theta rhythm. *Hippocampus* **3**, 317–330 (1993).
19. Mehta, M.R., Lee, A.K. & Wilson, M.A. Role of experience and oscillations in transforming a rate code into a temporal code. *Nature* **417**, 741–746 (2002).
20. Huxter, J.R., Senior, T.J., Allen, K. & Csicsvari, J. Theta phase–specific codes for two-dimensional position, trajectory and heading in the hippocampus. *Nat. Neurosci.* **11**, 587–594 (2008).
21. Ravassard, P. *et al.* Multisensory control of hippocampal spatiotemporal selectivity. *Science* **340**, 1342–1346 (2013).
22. Pastalkova, E., Itskov, V., Amarasingham, A., Buzsaki, G. & Buzsáki, G. Internally generated cell assembly sequences in the rat hippocampus. *Science* **321**, 1322–1327 (2008).
23. MacDonald, C.J., Lepage, K.Q., Eden, U.T. & Eichenbaum, H. Hippocampal "time cells" bridge the gap in memory for discontiguous events. *Neuron* **71**, 737–749 (2011).
24. Jezek, K., Henriksen, E.J., Treves, A., Moser, E.I. & Moser, M.-B. Theta-paced flickering between place-cell maps in the hippocampus. *Nature* **478**, 246–249 (2011).
25. Hahn, T.T.G., McFarland, J.M., Berberich, S., Sakmann, B. & Mehta, M.R. Spontaneous persistent activity in entorhinal cortex modulates cortico-hippocampal interaction *in vivo*. *Nat. Neurosci.* **15**, 1531–1538 (2012).
26. Miller, J.F. *et al.* Neural activity in human hippocampal formation reveals the spatial context of retrieved memories. *Science* **342**, 1111–1114 (2013).
27. Ekstrom, A.D. *et al.* Cellular networks underlying human spatial navigation. *Nature* **425**, 184–188 (2003).
28. Jacobs, J., Kahana, M.J., Ekstrom, A.D., Mollison, M.V. & Fried, I. A sense of direction in human entorhinal cortex. *Proc. Natl. Acad. Sci. USA* **107**, 6487–6492 (2010).
29. Rolls, E.T. Spatial view cells and the representation of place in the primate hippocampus. *Hippocampus* **9**, 467–480 (1999).
30. Dombeck, D.A., Harvey, C.D., Tian, L., Looger, L.L. & Tank, D.W. Functional imaging of hippocampal place cells at cellular resolution during virtual navigation. *Nat. Neurosci.* **13**, 1433–1440 (2010).
31. Harvey, C.D., Collman, F., Dombeck, D.A. & Tank, D.W. Intracellular dynamics of hippocampal place cells during virtual navigation. *Nature* **461**, 941–946 (2009).
32. Schmidt-Hieber, C. & Häusser, M. Cellular mechanisms of spatial navigation in the medial entorhinal cortex. *Nat. Neurosci.* **16**, 325–331 (2013).
33. Chen, G., King, J.A., Burgess, N. & O'Keefe, J. How vision and movement combine in the hippocampal place code. *Proc. Natl. Acad. Sci. USA* **110**, 378–383 (2013).
34. Cei, A., Girardeau, G., Drieu, C., El Kanbi, K. & Zugaro, M. Reversed theta sequences of hippocampal cell assemblies during backward travel. *Nat. Neurosci.* **17**, 719–724 (2014).
35. Hölscher, C., Schnee, A., Dahmen, H., Setia, L. & Mallot, H.A. Rats are able to navigate in virtual environments. *J. Exp. Biol.* **208**, 561–569 (2005).
36. Cushman, J.D. *et al.* Multisensory control of multimodal behavior: do the legs know what the tongue is doing? *PLoS ONE* **8**, e80465 (2013).
37. Aronov, D. & Tank, D.W. Engagement of neural circuits underlying 2D spatial navigation in a rodent virtual reality system. *Neuron* **84**, 442–456 (2014).
38. Hafting, T., Fyhn, M., Bonnevie, T., Moser, M.B. & Moser, E.I. Hippocampus-independent phase precession in entorhinal grid cells. *Nature* **453**, 1248–1252 (2008).
39. Mehta, M.R. Neuronal dynamics of predictive coding. *Neuroscientist* **7**, 490–495 (2001).
40. Cheng, J. & Ji, D. Rigid firing sequences undermine spatial memory codes in a neurodegenerative mouse model. *Elife* **2**, e00647 (2013).
41. Louie, K. & Wilson, M.A. Temporally structured replay of awake hippocampal ensemble activity during rapid eye movement sleep. *Neuron* **29**, 145–156 (2001).
42. Gelbard-Sagiv, H., Mukamel, R., Harel, M., Malach, R. & Fried, I. Internally generated reactivation of single neurons in human hippocampus during free recall. *Science* **322**, 96–101 (2008).
43. Hahn, T.T.G., McFarland, J.M., Berberich, S., Sakmann, B. & Mehta, M.R. Spontaneous persistent activity in entorhinal cortex modulates cortico-hippocampal interaction *in vivo*. *Nat. Neurosci.* **15**, 1531–1538 (2012).
44. Resnik, E., McFarland, J.M., Sprengel, R., Sakmann, B. & Mehta, M.R. The effects of GluA1 deletion on the hippocampal population code for position. *J. Neurosci.* **32**, 8952–8968 (2012).
45. Mehta, M.R. Contribution of Ih to LTP, place cells, and grid cells. *Cell* **147**, 968–970 (2011).
46. Russell, N.A., Horii, A., Smith, P.F., Darlington, C.L. & Bilkey, D.K. Lesions of the vestibular system disrupt hippocampal theta rhythm in the rat. *J. Neurophysiol.* **96**, 4–14 (2006).
47. Nitz, D.A. Path shape impacts the extent of CA1 pattern recurrence both within and across environments. *J. Neurophysiol.* **105**, 1815–1824 (2011).
48. Mehta, M.R., Quirk, M.C. & Wilson, M.A. Experience-dependent asymmetric shape of hippocampal receptive fields. *Neuron* **25**, 707–715 (2000).
49. Mehta, M.R., Barnes, C.A. & McNaughton, B.L. Experience-dependent, asymmetric expansion of hippocampal place fields. *Proc. Natl. Acad. Sci. USA* **94**, 8918–8921 (1997).
50. Mehta, M.R. & McNaughton, B.L. Expansion and shift of hippocampal place fields: evidence for synaptic potentiation during behavior. in *Computational Neuroscience Trends* (ed. Bower, J.) 741–745 (Plenum Press, New York, 1996).

ONLINE METHODS

Methods summary. The materials and methods used were similar to those described recently[21,36]. In brief, four adult male Long-Evans rats were trained to on a variety of tasks in RW and VR. All rats foraged for randomly scattered rewards in two-dimensional RW and VR environments. Additionally, three of these rats were trained to follow a goal-directed strategy by running toward randomly located reward-indicating pillars in VR. Further, the same three rats were trained to run toward consistently positioned reward locations in VR. There were either two or three fixed reward locations. The environments had identical dimensions (200-cm diameter circular platform at the center of a 300 cm × 300 cm room) and distal visual cues. Electrophysiological data from the dorsal CA1 were obtained using hyperdrives with 22 independently adjustable tetrodes[21]. Spike extraction and sorting were done offline using custom software. Spatial selectivity and phase precession were quantified using measures described previously[21]. Motifs were detected using custom analyses described in the main text. Further details are described below. Only data measured during locomotion (speed >5 cm s^{-1}) were used for all analyses to ensure consistent hippocampal state[51].

Subjects. Data were collected from four adult male Long-Evans rats (approximately 3.5 months old at the start of training) individually housed on a 12-h light, 12-h dark cycle and food restricted (15 g of food per day) to maintain body weight. The rats were allowed an unrestricted number of sugar-water rewards in VR but a restricted amount of water (~40 ml of water per day) after the behavioral session to maintain motivation. All experiments and data collection were performed during the light cycle. All experimental procedures were approved by the University of California Los Angeles Chancellor's Animal Research Committee and were conducted in accordance with US federal guidelines.

Random foraging in RW and VR. The experimental room, the VR apparatus and basic behavioral training were identical to those described recently[21,36]. In RW, a 200-cm-diameter and 50-cm-high platform was placed at the center of a 300 cm × 300 cm room with distinct visual cues on the four walls (**Fig. 1a**). Rats were trained to forage for randomly scattered food rewards on the platform. The VR room had an identical size and distal visual cues as the RW room, and rats foraged for randomly located rewards on a platform of the same size as that in the RW room. Rewards in VR were in the form of sugar water dispensed through reward tubes placed directly in front of the rats. The reward locations were hidden and were 40–60 cm in diameter. Entry into the reward locations triggered the appearance of a white dot of the same size on the platform in addition to a reward tone and sugar-water delivery. At each reward location, rats could receive a maximum of five sugar-water rewards. Motion parallax between the virtual elevated table and the floor underneath indicated the virtual edge of the platform. Movement beyond the platform edge resulted in no change in visual scene. Rats quickly learned to avoid or turn away from the virtual edges (**Fig. 1a**). It took about 3 weeks of handling and pretraining and 2 weeks of VR training for rats to do the random-foraging task efficiently. Rats were trained on the RW task after implantation. Three rats were run in both RW and VR every day. To verify that exposure to both worlds on the same day did not have a role in neural responses, a fourth rat never ran in both RW and VR on the same day. Further, the order of running in VR and RW on the same days was randomized. No qualitative differences were found between these conditions, and hence all data were combined.

Goal-directed tasks in VR. We trained three rats to run in three different goal-directed tasks: random pillar, two pillar and three pillar. In all of these tasks, the reward zone in VR space was indicated by a pillar suspended 50 cm above the table and a white dot on the table (**Fig. 3a**). All other variables, including the VR room, were identical to the one used for the random-foraging tasks. When rats reached the reward zone, the reward was dispensed, the pillar disappeared, and another pillar appeared elsewhere in the maze. Rats learned this task readily and ran toward the pillars reliably[36]. In the random-pillar task, a pillar appeared at a pseudorandom place in the two VR worlds. No qualitative differences were found between neural activity patterns in the random-pillar task and the random-foraging task, and hence these data were combined for subsequent analyses. In the two-pillar task, a pillar appeared alternately at one of two fixed places 160 cm apart in the middle of the VR table. In the three-pillar task, the reward-indicating pillar appeared sequentially at the vertices of an equilateral triangle with 138-cm-long sides centered on the VR platform.

Surgery, electrophysiology and spike sorting. These procedures were identical to those described earlier[21]. Briefly, once the rats reached performance criterion, they were anesthetized using isoflurane. Custom-made hyperdrives containing up to 22 independently adjustable tetrodes that targeted both the left and right dorsal CA1 were implanted. Rats were allowed to recover from surgery for 1 week, after which the tetrodes were gradually advanced to area CA1, detected online by the clear presence of sharpwave-ripple complexes. Spike and LFP data were recorded at 40 kHz using the Neuralynx acquisition system. Spikes were extracted and sorted into individual units using custom software. Classification of single-unit cell type was performed using the same methods as described previously[21]. When rats ran in both VR and RW on the same day, the same cells were identified by overlaying cluster boundaries from both sessions and identifying clear overlaps. If cell identities were unclear because of electrode drift, the data were discarded from the same cell analysis.

Statistics. Offline analyses were performed using custom MATLAB codes. Tests of significance between linear variables (circular variables) were done using the two-sided nonparametric Wilcoxon rank-sum test (Kuiper test). Tests of significance for the mean values of distributions being different from zero were performed using the two-sided nonparametric Wilcoxon signed-rank test. To compute circular statistics, the CircStat toolbox was used[52]. Tests of significance of correlation between two variables were done using a *t* test for correlation coefficients. All ensemble averages are in the form mean ± s.e.m. unless stated otherwise. All correlation values are reported as the linear correlation coefficient, *r*. A small number of single units were present in two different sessions, which could potentially inflate our estimate of the number of independent samples, thus altering the significance level of the statistical tests. Hence, as a conservative estimate, we did all tests of significance using only half as many cells in VR and RW. All significant results were still highly significant. No statistical methods were used to predetermine sample sizes, but our sample sizes are similar to those generally employed in the field. Data collection and analysis were not performed blind to the conditions of the experiments.

Quantification of rate maps. Theta rhythm is interrupted[51] and behavior is uncontrolled when rats pause to consume rewards or to groom. Hence, these periods were excluded, and only data recorded during periods of active locomotion (running speed >5 cm s^{-1}) were used. The durations of recording sessions were matched between RW and VR to remove possible sources of variability. A cell was considered active if its mean firing rate exceeded 0.2 Hz and it fired at least 100 spikes during locomotion, and such cells were thus included in the analysis. Spatial firing rates were computed using occupancy and spike histograms with 5 cm × 5 cm bins smoothed with a 7.5-cm two-dimensional Gaussian smoothing kernel. Bins with very low occupancy relative to the experimental session were excluded to avoid artificially high firing rates. The spatial information content, sparsity and coherence of the rate maps were computed using methods described previously[21]. To determine the stability of rate maps, firing rates were computed in the first and second halves of the session separately. The bin-by-bin correlation between the rate maps in the two halves provided a measure of rate map stability. To obtain the similarity of rate maps of the same cell in RW and VR, we computed the correlation of firing rates and computed statistical significance by comparing it against correlations when the cell identities were shuffled.

Computation of dynamic rate maps. The dynamic rate map[53] for a pair of coactive cells was constructed as follows: for each spike from the first cell, the rat trajectory and spikes from the second cell within the next 200 cm traveled were aggregated relative to the spike positions from the first cell. We used 15 cm × 15 cm spatial bins and computed the occupancy time and number of spikes in each bin. Dividing the number of spikes by the occupancy time in each spatial bin provided the dynamic rate map. The information content and sparsity of these rate maps were quantified as described above.

Computation of coactivation of cell pairs. To determine the degree of coactivity of pairs of cells active in a session, we first constructed the firing rate of neurons as a function of both time elapsed and distance traveled (200 ms (5 cm) time

(distance) bins, smoothed with a 400 ms (10 cm) Gaussian smoothing kernel). We then computed the cross-covariance of firing rates for pairs of active cells within a session. To obtain an estimate of chance level, we generated control data by time reversing the spike train of one of the cells in the cell pair and time shifting both of them by random amounts between 10 and 100 s. This procedure was repeated ten times. We detected the peak value in the cross-covariance of the original cell pairs and the control data in both distance and time domains $\left(\text{peak}_{\text{actual}}^{\text{distance}}, \text{peak}_{\text{control}}^{\text{distance}} \text{ and } \text{peak}_{\text{actual}}^{\text{time}}, \text{peak}_{\text{control}}^{\text{time}}\right)$ that occurred within 50 cm or 2 s from 0. A peak was considered significant if it satisfied the following condition:

$$\text{peak}_{\text{actual}}^{\text{distance}} \geq \text{mean}\left(\text{peak}_{\text{control}}^{\text{distance}}\right) + 2 \times \text{standard deviation}\left(\text{peaks}_{\text{control}}^{\text{distance}}\right)$$

$$\text{peak}_{\text{actual}}^{\text{time}} \geq \text{mean}\left(\text{peak}_{\text{control}}^{\text{time}}\right) + 2 \times \text{standard deviation}\left(\text{peaks}_{\text{control}}^{\text{time}}\right)$$

We then calculated the fraction of cell pairs whose firing rate cross-covariance had a significant peak.

Characterizing selectivity to distances traveled in VR goal-directed tasks. To investigate the degree of selectivity to distance traveled in the goal-directed tasks (VR systematic-pillar and VR random-pillar tasks), we linearized the paths by measuring the distance traveled between two consecutive rewards. These distances were normalized to unity. To control for variability in the path lengths, we considered only trials for which the distance traveled was around the median path length (median ± 0.4 × median). This threshold value of 0.4 ensured that the number of trials and path-length variability were similar in the random-pillar and systematic-pillar tasks. The following analysis was also repeated when considering all trials regardless of the path lengths, and the results were qualitatively similar. For each cell, we constructed a linearized rate map as a function of the normalized distance traveled. For cells with a mean firing rate above 0.5 Hz, we then computed the information content, sparsity and peak value of the rate maps to quantify this selectivity. To examine the nature of this selectivity on an ensemble level, for each cell we partitioned the selected trials into two random groups. We computed the firing rate for each partition separately. The population vector overlap for the two partitions was calculated, and the significance values were obtained using methods described previously[26].

Computation of disto-code in the VR three-pillar task. Here, a one-dimensional linearized rate map was constructed (distances were normalized to unity) for each arm separately. A given arm pair was used for analysis if the mean firing rate was higher than 0.5 Hz on at least one arm. We then computed the arm selectivity index for each two-arm combination as

$$D_{ij} = \left| \frac{\sum_l^L (\lambda_l^i - \lambda_l^j)}{\sum_l^L (\lambda_l^i - \lambda_l^j)} \right|$$

where λ_l^i and λ_l^j are the rates in the l^{th} bin along arms i and j. For the arm pairs with $D < 0.5$ (pairs with firing along both arms), we computed the population vector overlap, its significance level and disto-coding index similarly to methods described previously[26].

Detection of motifs. To detect motifs, a method similar to the one used for detecting place fields on a one-dimensional track was used. We constructed a spike train, a vector of data whose length spanned the period of the experimental session, by binning the spikes for which the running speed was greater than 5 cm s^{-1}. This spike train was smoothed using a 200-ms Gaussian smoothing kernel and transformed to firing rate by dividing by the bin duration. Peaks where the firing rate exceeded 5 Hz were detected and marked as candidate motifs. The boundaries of a motif were defined as the points where the firing rate first dropped below 10% of the peak rate (within the motif) for at least 250 ms (two theta cycles). If the time lag between the first and last spike in the putative motif, called the duration of the motif, exceeded 300 ms, this sequence was considered a valid motif and was included in the analysis.

Construction of motif fields. The center of a motif was defined as the center of mass of the firing rate as a function of time within the motif. This value was subtracted from the spike times within the motif to center them around zero. This procedure was repeated for all motifs, and the centered motifs were aligned to obtain a motif field for a given neuron. The firing rate as a function of time within the motif field was calculated as the number of spikes within each temporal bin divided by the total amount of time in that bin, smoothed by a 200-ms Gaussian smoothing kernel. Motif-field duration was defined as twice the weighted s.d. of the motif firing rate, i.e., the width of the distribution.

Theta period and phase precession. Similar to the methods described previously[21], each LFP was filtered between 4 and 12 Hz using a fourth order Butterworth filter. Theta period was computed by detecting the peak between 50 and 200 ms in the filtered LFP autocorrelation for epochs during which the running speed was above 5 cm s^{-1}. Spiking theta period was calculated by computing the spike train autocorrelation, smoothing by a 15-ms-wide Gaussian kernel and detecting the peak. Quality of phase precession within a motif field was defined as the circular linear correlation coefficient (CLCC)[21] between spike phases and the latency of spike timing with respect to the motif center.

Control analysis for motifs. To estimate which motif properties can arise purely by chance, surrogate motifs for each neuron were generated as follows. The mean firing rate during locomotion and the depth of theta modulation were computed for each neuron. Surrogate activity was generated using a Poisson-distributed and theta-modulated spike train with the same mean firing rate and depth of theta modulation as the experimentally measured neuron. Motifs, motif fields and their properties were computed using the procedures described above. This procedure was repeated 50 times for each neuron to generate a null distribution. The mean value and s.d. of this null distribution were used to compute the z-scored values for each cell.

Control analysis for spatial selectivity. To determine the statistical significance of spatial selectivity, we generated control data by shifting the experimentally observed spike train with respect to behavioral data by random amounts between 10 and 100 s. All of the measures used to quantify the spatial selectivity were expressed in the units of z score or s.d. around the control data.

A **Supplementary Methods Checklist** is available.

51. Vanderwolf, C.H. Hippocampal electrical activity and voluntary movement in the rat. *Electroencephalogr. Clin. Neurophysiol.* **26**, 407–418 (1969).
52. Berens, P. CircStat: a MATLAB toolbox for circular statistics. *J. Stat. Softw.* **31**, 1–21 (2009).
53. Bonnevie, T. *et al.* Grid cells require excitatory drive from the hippocampus. *Nat. Neurosci.* **16**, 309–317 (2013).

doi:10.1038/nn.3884

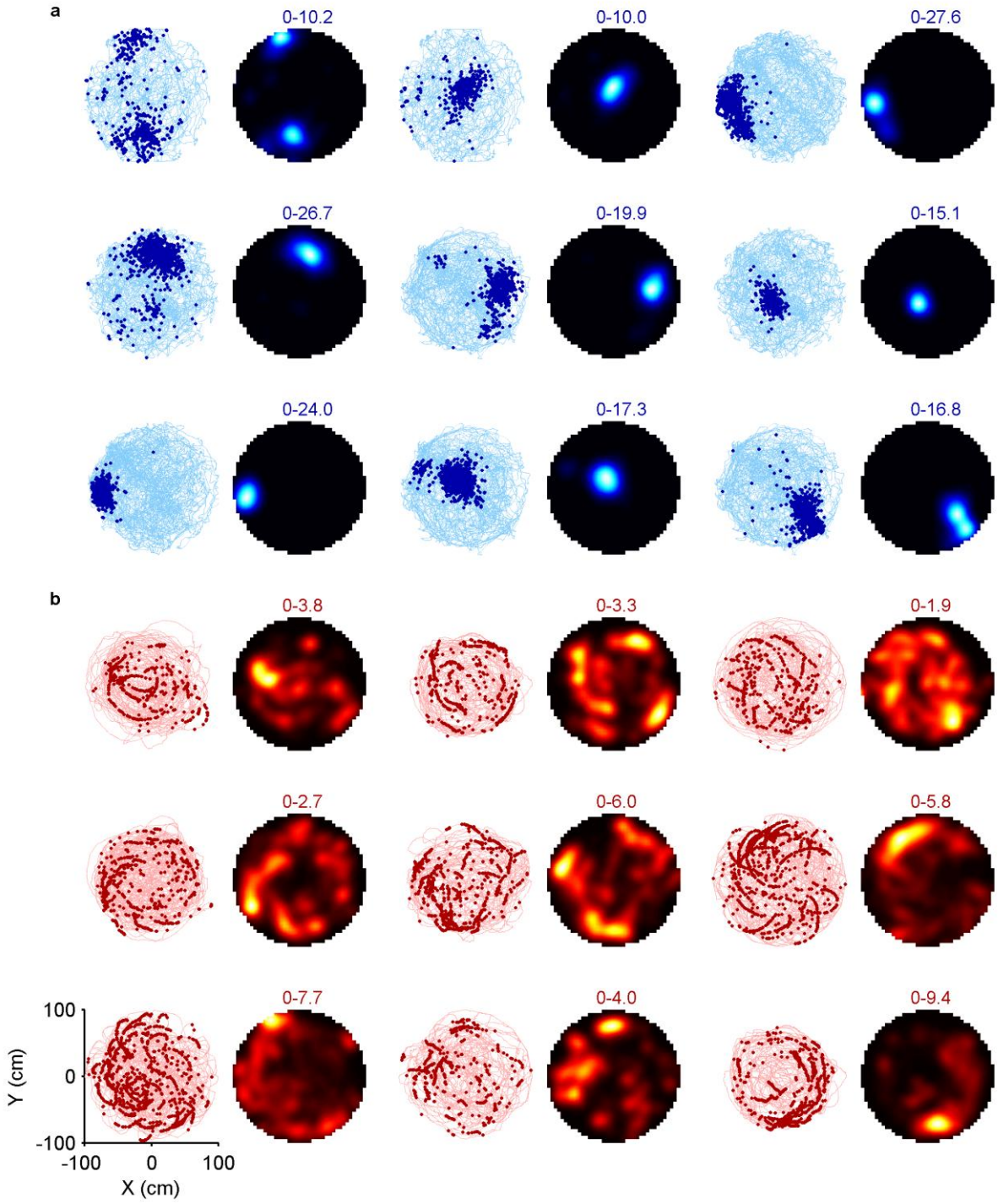

Supplementary Figure 1

Additional example cells in RW and VR showing lack of spatial selectivity in VR.

a, Rat trajectory and spike positions for different neurons and corresponding firing ratemaps in RW. **b,** Same as (**a**) but in VR, showing long streaks of spikes, or putative motifs. Numbers indicate firing rate range. Color conventions are the same as in Fig. 1.

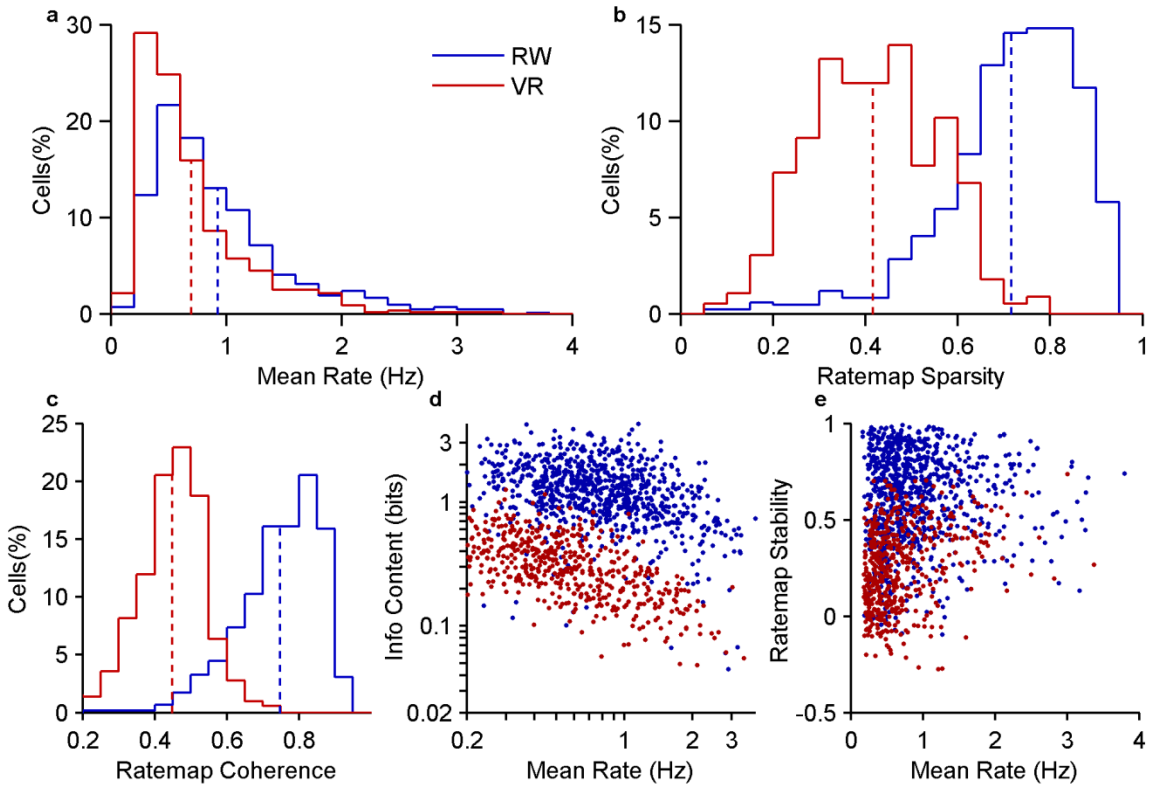

Supplementary Figure 2

Reduced mean firing rates, rate map sparsity and coherence in VR.

a, Mean firing rates were 25% ($p=7.6\times10^{-20}$) lower in VR (0.70±0.02Hz) than in RW (0.93±0.02Hz). **b,** Ratemap sparsity, a measure of spatial selectivity, was also greatly (42%, $p=2.3\times10^{-162}$) reduced in VR (0.42±0.01) compared to RW (0.72±0.01). **c,** Ratemap coherence computed using 10x10cm bins, was 40% ($p=2.3\times10^{-157}$) reduced in VR (0.45±0.01) compared to RW (0.75±0.01). **d,** At all mean rates, spatial information content was negatively correlated with the mean firing rate of a cell in both worlds (RW r=-0.36, $p=1.6\times10^{-27}$; VR r=-0.48, $p=3.2\times10^{-33}$). **e,** Spatial stability was lower in VR compared to RW. Stability was not correlated with mean firing rate in RW (r=0.02, p=0.54) and weakly positively correlated in VR (r=0.28, $p=1.1\times10^{-11}$).

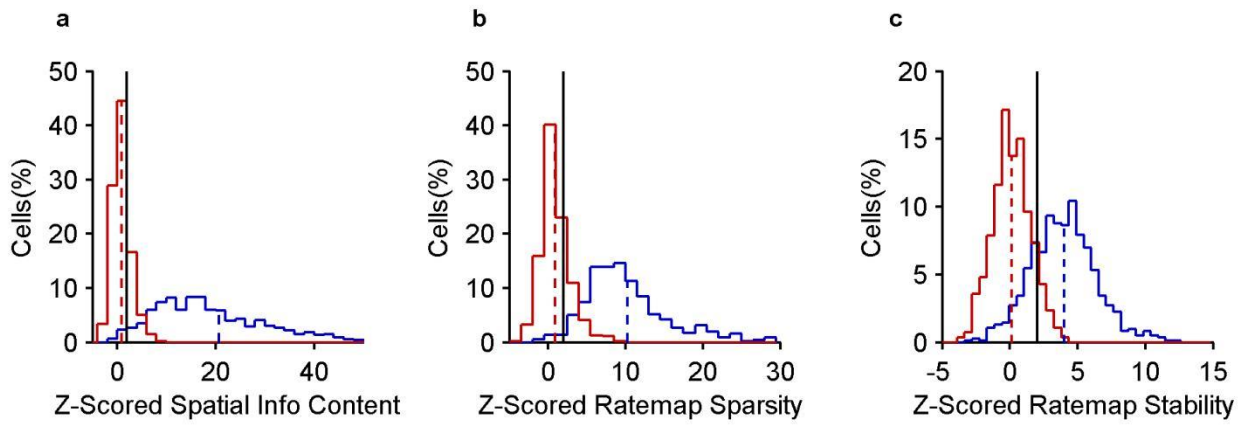

Supplementary Figure 3

Estimation of the significance levels of spatial selectivity showing VR results were near chance levels.

To quantify spatial information content, ratemap sparsity and stability that are uninfluenced by the mean firing rate of a cell, these were computed in Z-scored units for each cell (see Methods). **a,** Z-scored spatial information content was only slightly greater than zero in VR (0.92±0.08, $p=3.2\times10^{-27}$) but the difference was far greater in RW (20.65±0.49, $p=7.7\times10^{-140}$), and the two distributions were significantly different (difference=19.73, $p=7.4\times10^{-206}$). **b,** Similar to information content, Z-scored ratemap sparsity was only slightly greater than zero in VR (0.91±0.07, $p=3.4\times10^{-32}$) but the difference was far greater in RW (10.26±0.20, $p=7.7\times10^{-140}$). These two distributions were significantly different (difference=9.35, $p=9.5\times10^{-200}$). **c,** The Z-scored stability was close to zero in VR (0.13±0.06, p=0.036) but significantly above chance in RW (3.99±0.09, $p=1.0\times10^{-135}$; difference=3.86, $p=1.2\times10^{-155}$).

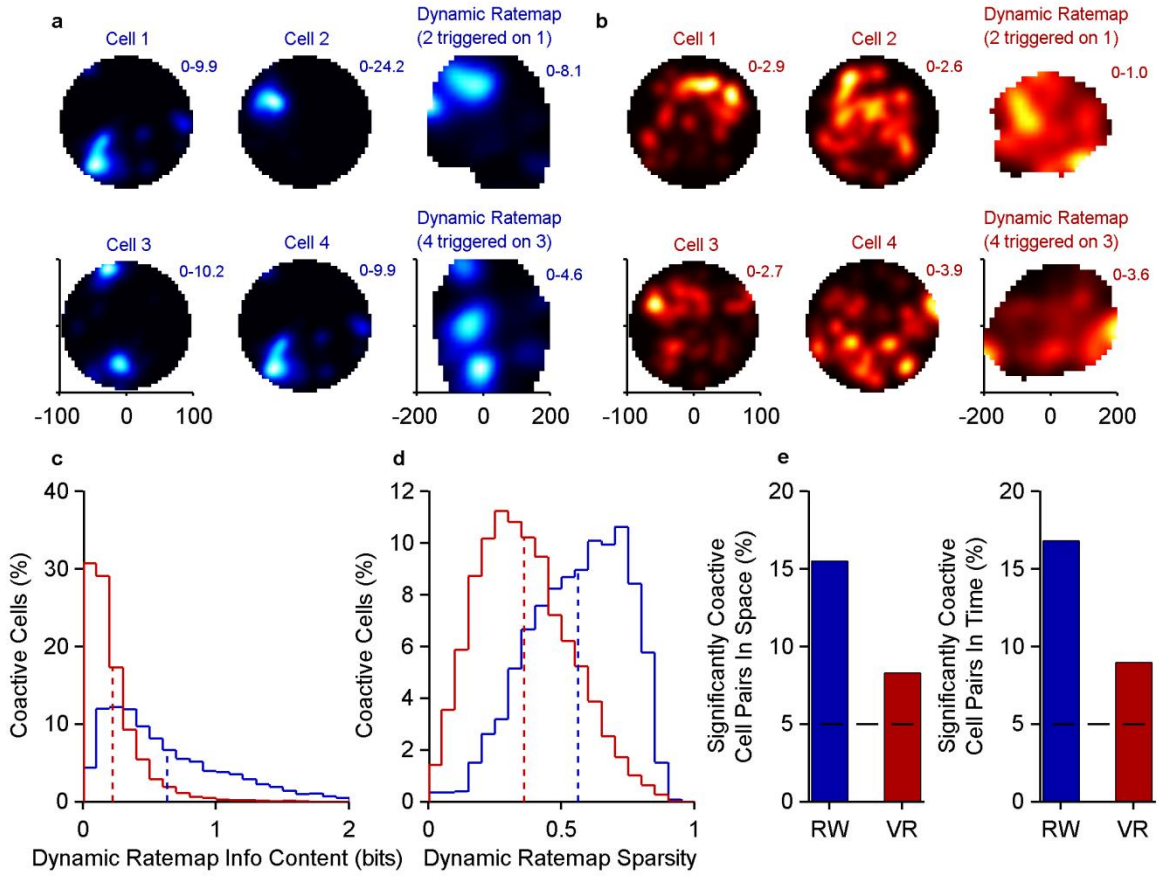

Supplementary Figure 4

Loss of spatial selectivity in dynamic rate maps and reduction in neuronal coactivation in VR.

a, Spatial ratemaps of two pairs of neurons in RW (left) and their dynamic ratemap (right) (see Methods) showing spatially localized activity. Numbers on top right indicate firing rate range. **b,** Same as (**a**) but for two pairs of neurons in VR showing no spatial selectivity. **c,** Dynamic ratemap information content in RW (0.63±0.01bits, n=10831 pairs from 4 rats) was 65% greater ($p<10^{-100}$) than in VR (0.22±0.00bits, n=8202 pairs from 4 rats). **d,** Dynamic ratemap sparsity in RW (0.56±0.002) was also greater (36%, $p<10^{-100}$) than in VR (0.36±0.002). The relative spiking of coactive neurons was spatially informative in RW but not in VR. **e,** In order to investigate coactivity of cell pairs (including sequential activity on intermediate time- and length scales) we computed cross-covariances between the firing rates of pairs of active cells in a session as a function of time elapsed or distance traveled (see methods). The fraction of coactive cells in RW (15.5(16.8)% in distance(time) domain) was far greater than that in VR (8.3(8.9)% in distance(time) domain).

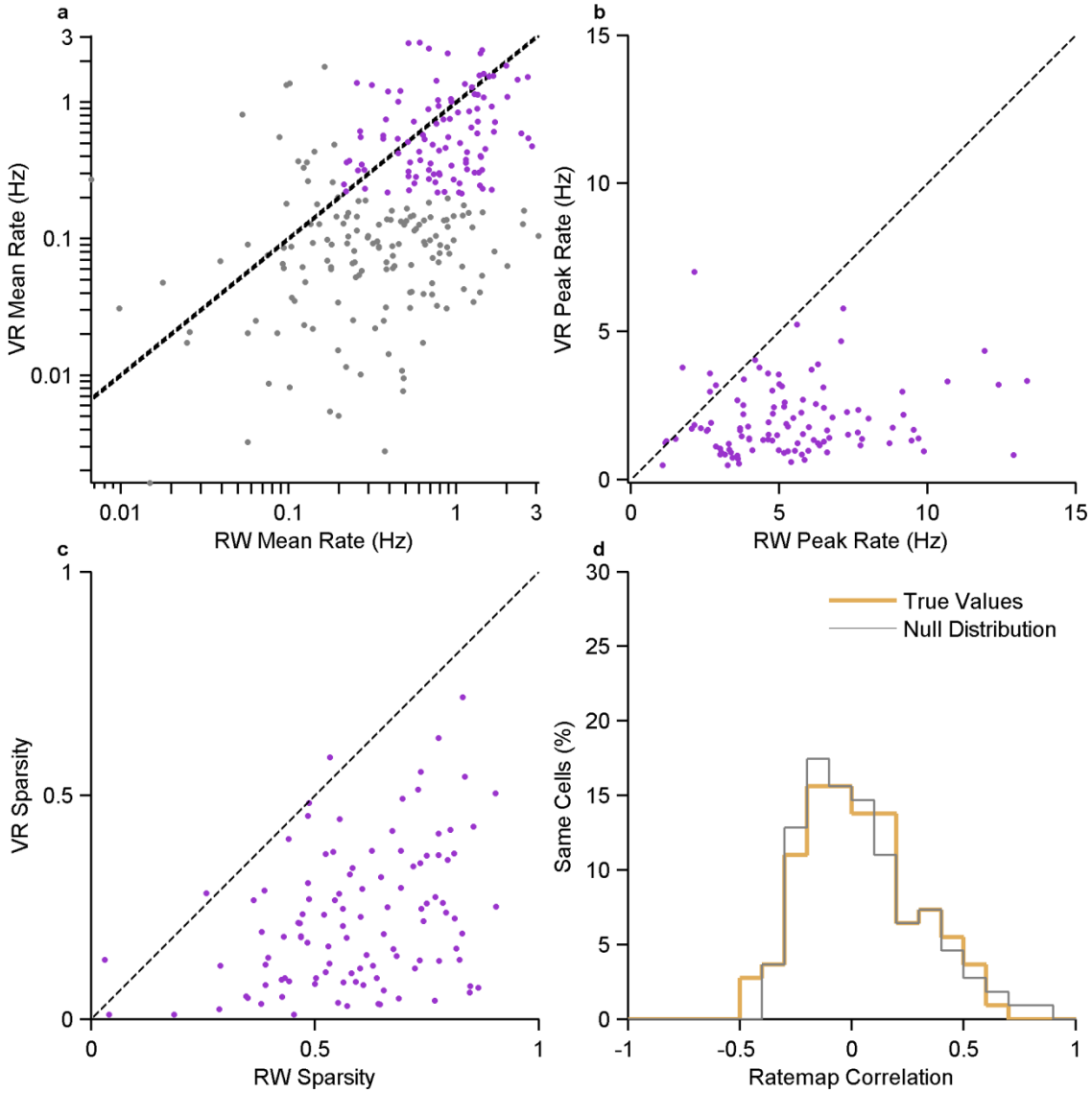

Supplementary Figure 5

Comparison of activities of cells active in both RW and VR on the same day.

a, For cells recorded in both worlds on the same day mean firing rate was correlated regardless of minimum firing rate (grey, r=0.32, $p=1.7x10^{-7}$, n = 258 from 3 rats). This was also true for the subset of cells active at high rates in both worlds (purple, r=0.21, p=0.03, n = 109 from 3 rats), used for all subsequent same-cell analyses. **b,** The peak firing rate of the same cell was reduced in VR compared to RW and the two were not significantly correlated (r=0.12, p=0.23), despite their correlated mean rates, due to lack of spatial selectivity in VR. **c,** Spatial ratemap sparsity of the same cell was also reduced in VR but correlated with RW (r=0.36, p=0.0001), which could be partially explained by correlated mean firing rates (Fig. 2e). **d,** Despite positive correlations in mean rate and sparsity, the distribution of correlation of ratemaps of the same cells between RW and VR is not significantly different from zero (p=0.39) and not different from the ratemap correlations obtained by shuffling the cell identities (p=0.97).

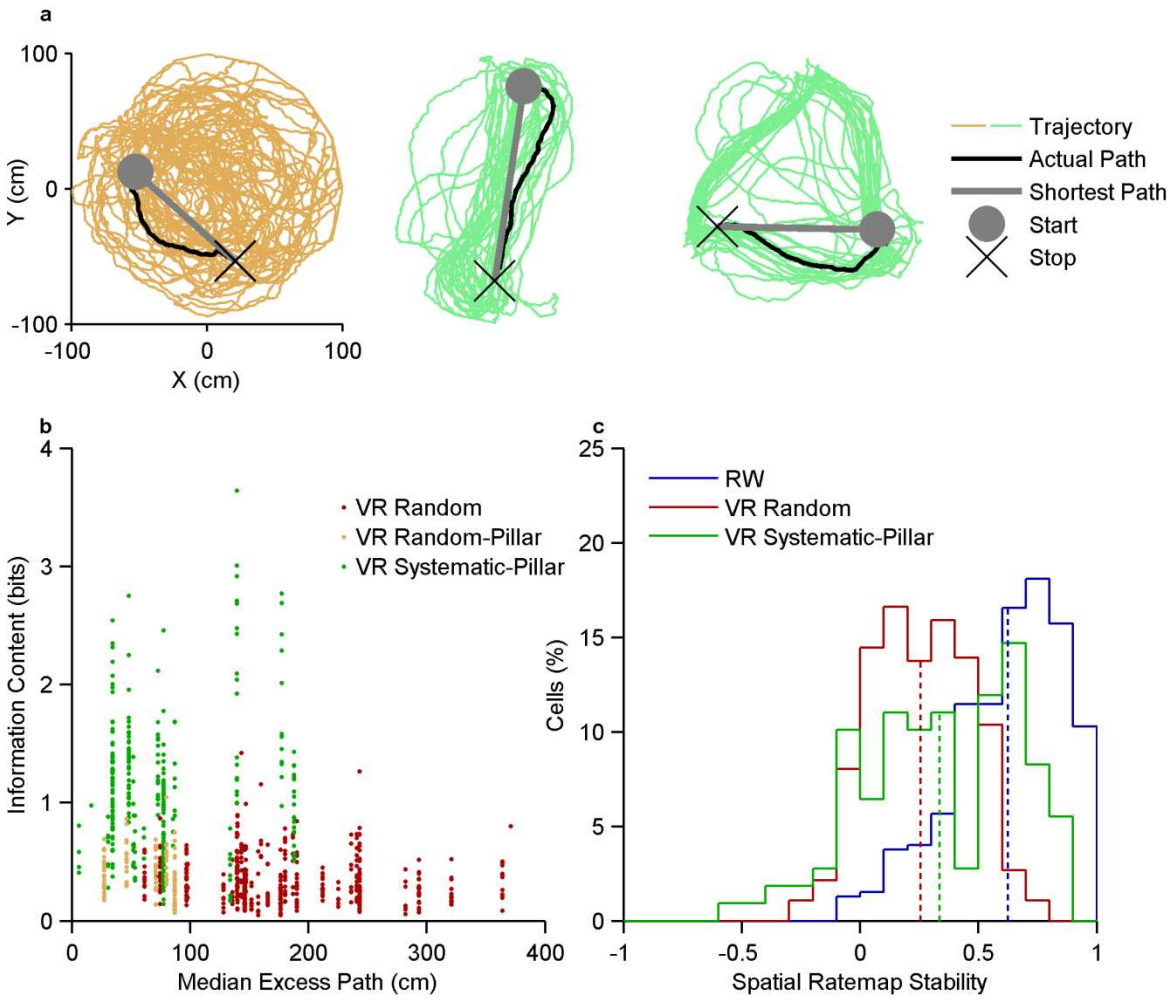

Supplementary Figure 6

Quantification of behavior and neural responses during goal-directed VR tasks.

a, Rats' sample trajectories between two reward locations and the corresponding shortest path between them in the VR random-pillar task (left) and VR systematic-pillar tasks (center and right). **b,** We defined the excess path length as the difference between the shortest distance between two consecutive reward locations and the actual path length traveled by the rat. We then calculated the median value of this excess path length over an entire session. The rats' behavior was more goal-directed during the VR random-pillar task because the median excess path length (56.3 ± 10.8 cm) was significantly smaller compared to random foraging task (178.2 ± 13.9 cm, $p = 6.1 \times 10^{-4}$). A similar effect was observed in VR systematic-pillar where the median excess path length (77.3 ± 12.2 cm) was significantly shorter compared to random foraging (178.2 ± 13.9 cm, $p = 1.4 \times 10^{-5}$). Further, VR random-pillar and VR systematic-pillar were equally goal-directed because the median excess path lengths were comparable in the two conditions ($p = 0.44$). **c,** Ratemap stability in the VR systematic-pillar task (0.34 ± 0.03, n = 282 cells with at least 100 spikes in each session half from 3 rats) is greater than VR random foraging ($p = 2.4 \times 10^{-3}$) and smaller than RW random foraging ($p = 1.8 \times 10^{-18}$).

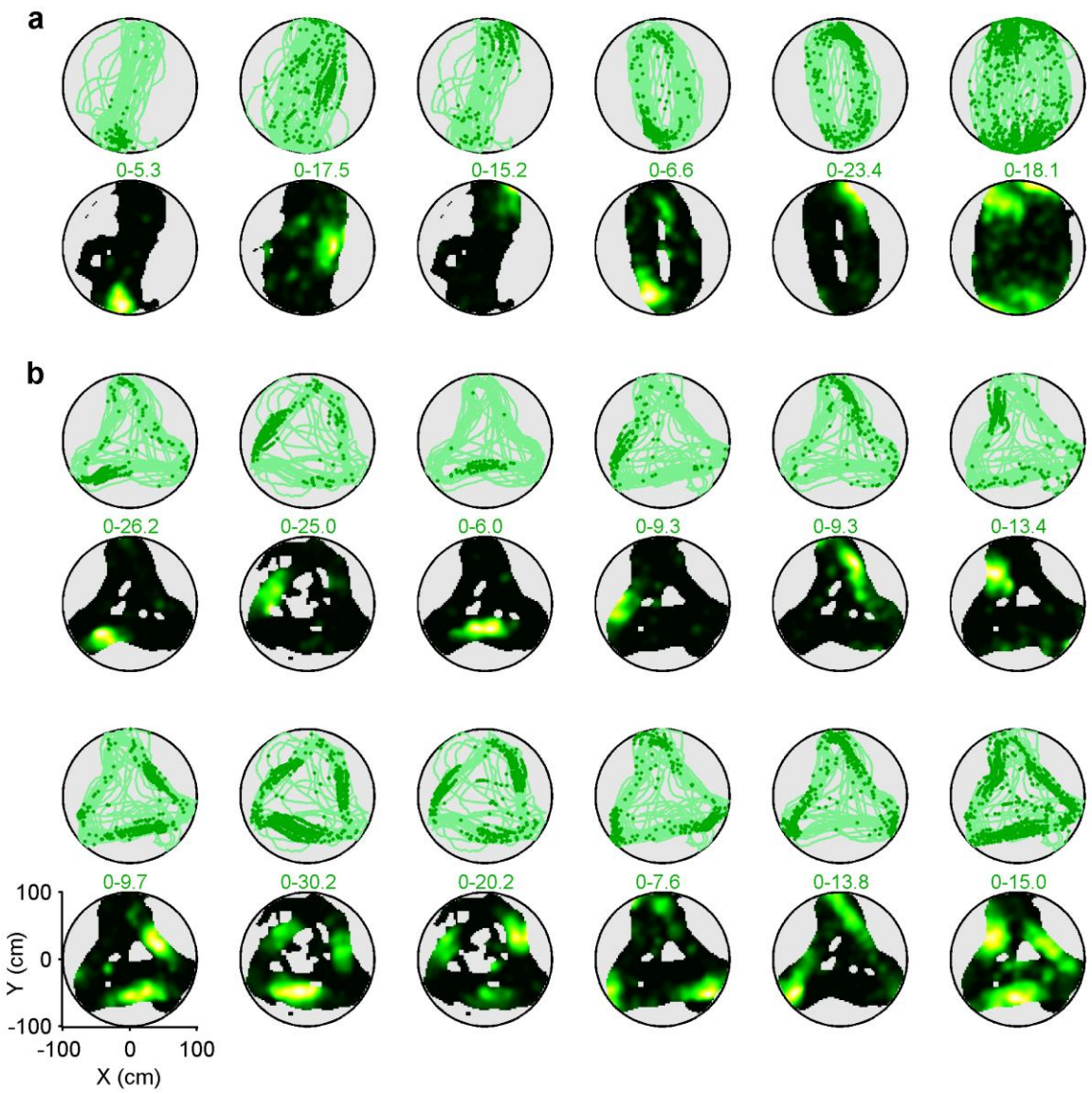

Supplementary Figure 7

Additional example cells in VR in systematic-pillar tasks.

a, Rat trajectory and spike positions for different neurons (top row) and corresponding firing ratemaps (bottom row) for the two-pillar task. **b,** Same as (**a**) but for the three-pillar task. Numbers indicate firing rate range. Color conventions are the same as in Fig. 3. Note that examples show elevated firing along only one or multiple arms of the triangle.

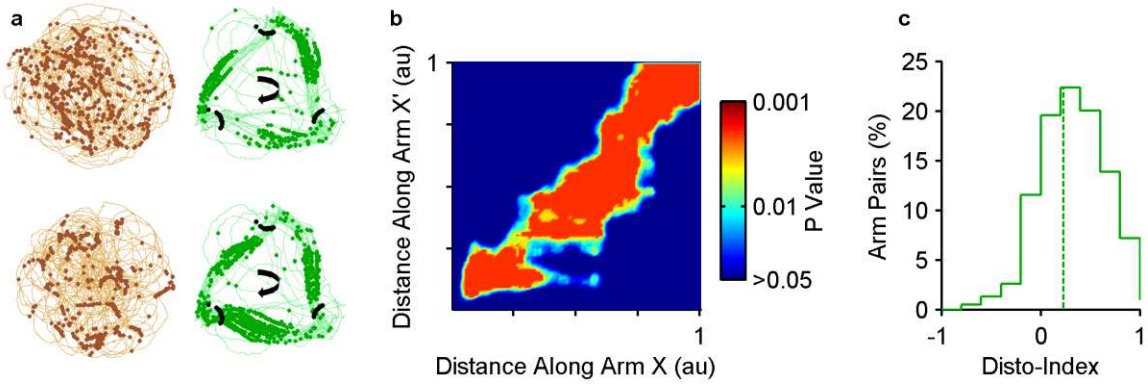

Supplementary Figure 8

Selectivity to distance traveled in VR goal-directed tasks and presence of disto-code in the three-pillar task.

a, Left: Trajectory of the rat (light brown) and spike positions (dark brown) during the VR random-pillar task on the two-dimensional platform for the same cells shown in Fig. 4a. Note that the cells fire randomly in two-dimensions although one of them (bottom panel) does exhibit selectivity to distance along the linearized path. Right: Same as left but for VR systematic-pillar task (trajectory and spikes are depicted in light and dark green respectively). The black dots indicate the reward locations and the arrows correspond to running direction. **b,** Significance levels (p values) for population vector overlap in Fig. 4d. The significant diagonal is indicative of firing at the same distance along the two arms (disto-coding). **c,** Disto-coding index (see Methods) for the population of multi-arm selective arm pairs (n = 431 arm pairs from 3 rats) in the three-pillar task was also significantly positive (0.23±0.02 ,$p=1.5x10^{-31}$), further supportive of a disto-code.

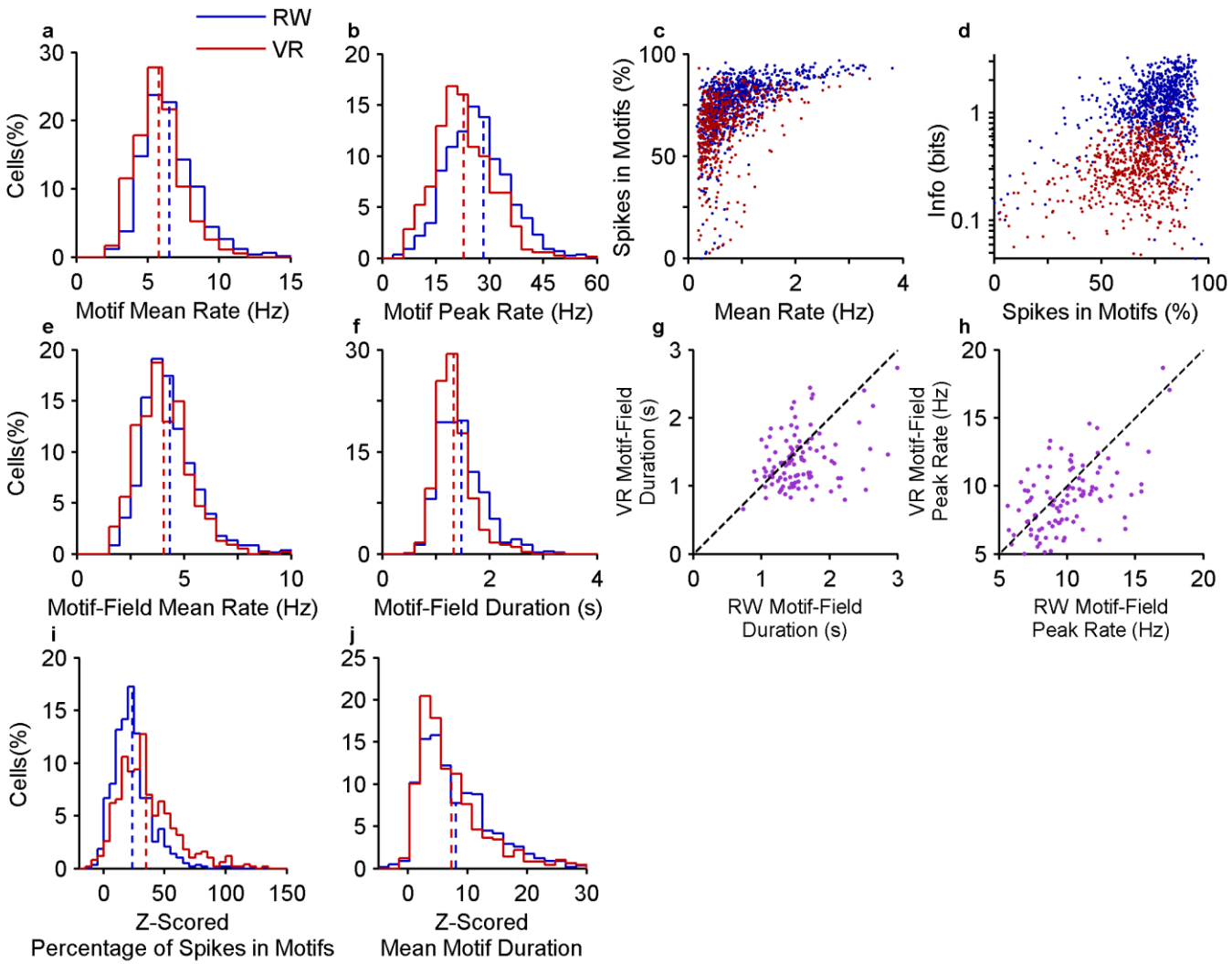

Supplementary Figure 9

Comparable spatiotemporal properties of individual motifs and motif fields in RW and VR.

a, For each cell we computed the mean firing rate within individual motifs and calculated the mean of those values to obtain a single number for individual cells. Motif mean rates in VR (5.92±0.06Hz) were slightly smaller (10%, $p=7.7\times10^{-10}$) than in RW (6.52±0.06Hz). **b,** Similarly, motif peak rates in VR (23.39±0.24Hz) were smaller (21%, $p=6.1\times10^{-21}$) than in RW (28.32±0.69Hz). **c,** There was significant correlation between mean rate and the percentage of spikes that occurred within motifs in RW ($r=0.54$, $p=4.1\times10^{-65}$) and VR ($r=0.41$, $p=1.2\times10^{-28}$). This could explain the reduced motif duration and percentage of spikes contained in motifs in VR compared to RW (Fig. 5e). **d,** In both RW and VR, the percentage of spikes in motifs was significantly correlated with spatial information content of a neuron (RW $r=0.28$, $p=4.2\times10^{-17}$; VR $r=0.26$, $p=6.5\times10^{-12}$). **e,** Motif-field mean firing rates in VR (4.12±0.05Hz) were only slightly smaller (5%, $p=9.2\times10^{-3}$) than in RW (4.34±0.05Hz). **f,** Motif-field durations in VR (1.33±0.01s) were similar but slightly reduced (10%, $p=1.1\times10^{-12}$) compared to RW (1.48±0.01s). **g,** For cells active in both worlds on the same day, motif-field duration was correlated between RW and VR ($r=0.31$, $p=1.2\times10^{-3}$). **h,** Motif-field peak firing rate had a similar correlation ($r=0.54$, $p=1.2\times10^{-9}$). **i, j,**To estimate the percentage of spikes contained in motifs and motif durations, uninfluenced by the mean rate, we computed the Z-scored values for these two measures (see Methods). **i,** The Z-scored percentage of spikes in motifs was significantly above zero in VR (35.15±1.06, $p=3.9\times10^{-83}$) and RW (23.52±0.64, $p=1.0\times10^{-26}$). In fact larger Z-scored values in VR indicate greater propensity for motif generation compared to RW. **j,** The Z-scored mean motif duration was indeed similar in both worlds (8.02±0.25 in RW and 7.33±0.27 in VR, $p=0.03$) and greatly above zero ($p=2.1\times10^{-96}$ and $p=1.4\times10^{-83}$ in RW and VR respectively).

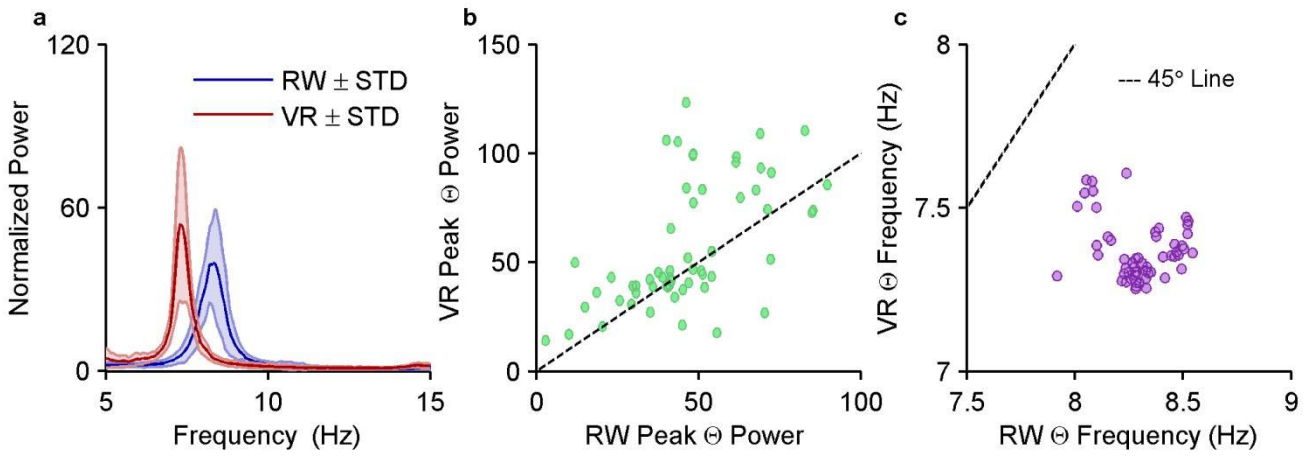

Supplementary Figure 10

Increased theta power but reduced theta frequency in VR.

To further examine the dynamics of LFP theta, we investigated the LFPs recorded from the same electrode on the same day in both worlds without any electrode movement between the two sessions. Analysis was further restricted only to data when rats ran at speeds greater than 5cm/s to eliminate contamination by variable periods of stopping when theta is reduced. In order to compare data from different sessions, the power spectrum from each electrode was normalized by the mean power on that electrode in RW and VR over the frequency range 1-100 Hz.

a, Normalized power between 5-15 Hz, averaged over all the LFP (n=57 from 3 rats) in RW and VR shows a clear difference in theta power and frequency between the two environments. **b,** Peak theta power is significantly increased ($p=0.002$, paired Wilcoxon signed rank test) in VR (56.95±3.75) compared to RW (46.61±2.51). **c,** Theta frequency in VR (7.21±0.07Hz) is significantly lower ($p=5.1\times10^{-11}$) than in RW (8.32±0.06Hz).